Presented at the Conference on the
Properties of Nuclei Far from the
Region of Beta Stability, Leysin,
Switzerland, August 31-September 4, 1970

UCRL-19961
Preprint

HEAVY-ION IN-BEAM SPECTROSCOPY

R. M. Diamond

August 1970

AEC Contract No. W-7405-eng-48

LAWRENCE RADIATION LABORATORY
UNIVERSITY of CALIFORNIA BERKELEY

UCRL-19961

DISCLAIMER

HEAVY-ION IN-BEAM SPECTROSCOPY

R. M. Diamond

Lawrence Radiation Laboratory
University of California
Berkeley, California 94720

1. INTRODUCTION

In-beam gamma-ray and conversion-electron spectroscopy has certainly come of age in the four years since the Lysekil Conference on "Nuclides far off the Stability Line." Not only have techniques become more refined, involving pulsed beams and multi-dimensional coincidence studies, but many laboratories are now actively engaged in this type of work or are about to plunge in. The use of heavy-ion beams offers several features that can be exploited to advantage, namely; 1) high projectile nuclear charge, indispensible for multiple Coulomb excitation work; 2) large linear momentum transfer, helpful in Doppler-shift, IMPACT, and other recoil studies; 3) large angular momentum transfer, useful in the production of high-spin states and isomers and of highly aligned product nuclei; 4) good product specificity while still permitting a wide range of neutron-deficient nuclei to be studied.

I shall illustrate these features with examples of heavy-ion in-beam studies, mostly taken from work at the Berkeley HILAC. These will be grouped into three categories dealing with I) Nuclear moments, II) Energy level systematics, and III) How neutron deficient can we get?

2. NUCLEAR MOMENTS

2.1. Electric moments

The principal electric transition moment studied to-date has been the reduced quadrupole moment or B(E2). It can be determined by direct half-life measurement or by Coulomb excitation. The advent of high-

resolution Ge(Li) detectors has had an impact on all types of measurements, but in particular has made the recoil-distance Doppler-shift method[1-5] a most useful one for the important half-life region between 10^{-10} and 10^{-12} seconds. The power of this method has been demonstrated by Alexander and Allen[6,7] and others[8-11]. In addition, the use of heavy-ion projectiles to (Coulomb) excite the levels to be measured results in a larger recoil velocity, thus permitting a thicker target (higher yield) and a more accurate measurement[12,13]. The principle of the latter scheme is shown in Fig. 1. The nucleus recoiling from the back-scattered projectile may decay in flight (shifted peak) or after being stopped in the plunger (unshifted peak). The fraction of gamma-ray intensity (in coincidence with back-scattered ^{40}Ar ions) that is unshifted in energy, F_u, is approximately $e^{-\frac{d}{v\tau}}$, where d is the target-plunger distance, v is the velocity of the recoiling nucleus, and τ is the mean-life of the excited state being measured. The velocity, $v = \beta c$, is determined from the Doppler-shift itself using

$$\frac{\Delta E}{E_0} = \frac{(1-\beta^2)^{1/2}}{\beta(1-\cos\theta_c)} \ln\left(\frac{(\beta+1)(1-\cos\theta_0)}{\beta\cos\theta_c-\cos\theta_0 + [(\cos\theta_0-\beta\cos\theta_c)^2+(1-\beta^2)\sin^2\theta_0]^{1/2}}\right) - 1 \quad . \quad (1)$$

Thus a number of measurements of F_u at various distances, d, (Fig. 2) yield a plot (Fig. 3) from which τ is obtained by a computer best-fit. A number of small corrections have to be made, as well as allowance for feeding from higher-lying states, and for the gamma-ray angular distribution and its attenuation[10,12].

The results of such a study for the ground-state band in ^{152}Sm are shown in Table 1 (Ref. 13). The experimental B(E2) values are somewhat

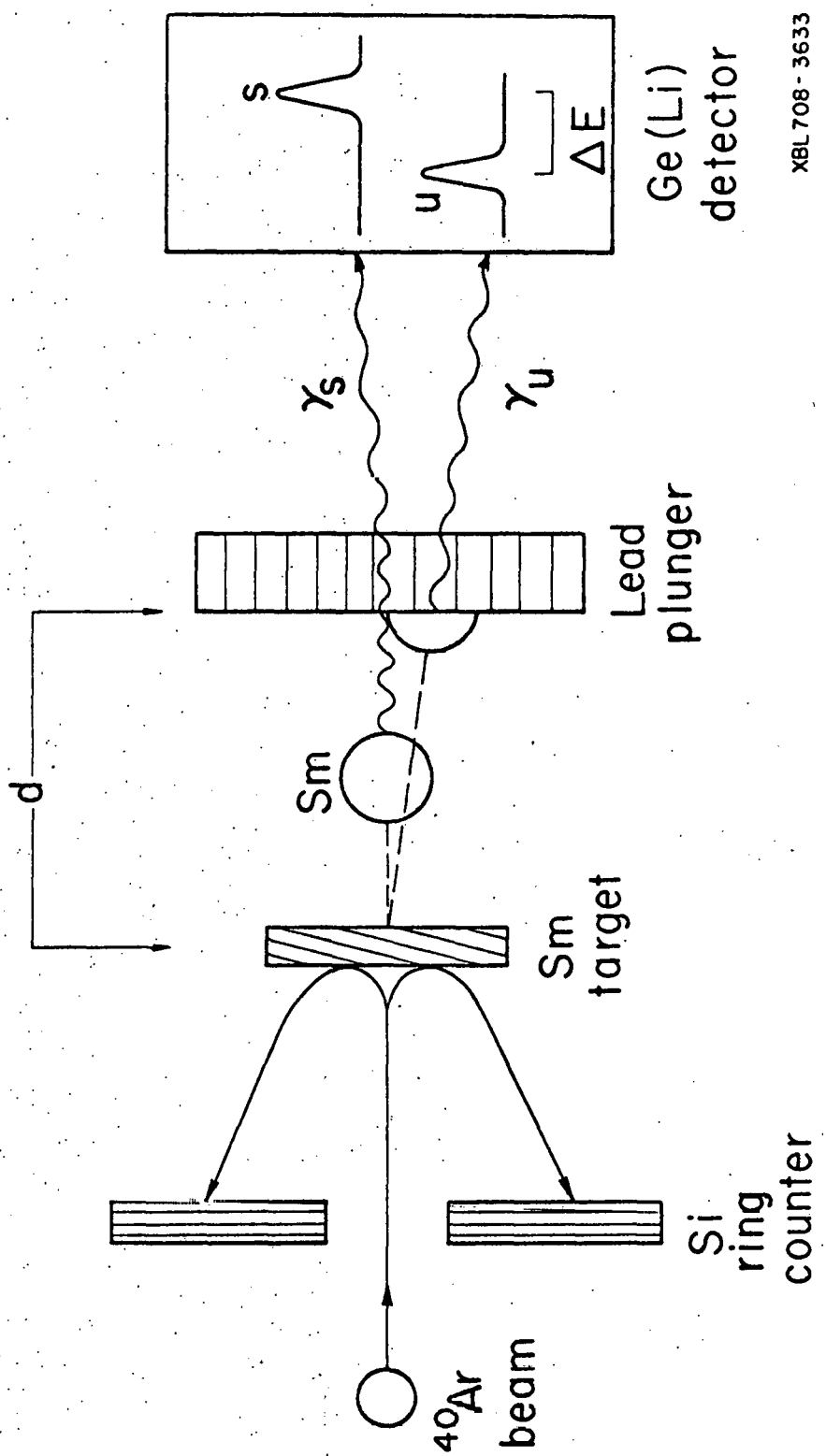
s
u
ΔE
Ge(Li)
detector
XBL 708-3633
γ_s
γ_u
Lead
plunger
d
Sm
Sm
target
Si
ring
counter
^{40}Ar
beam

Fig. 1

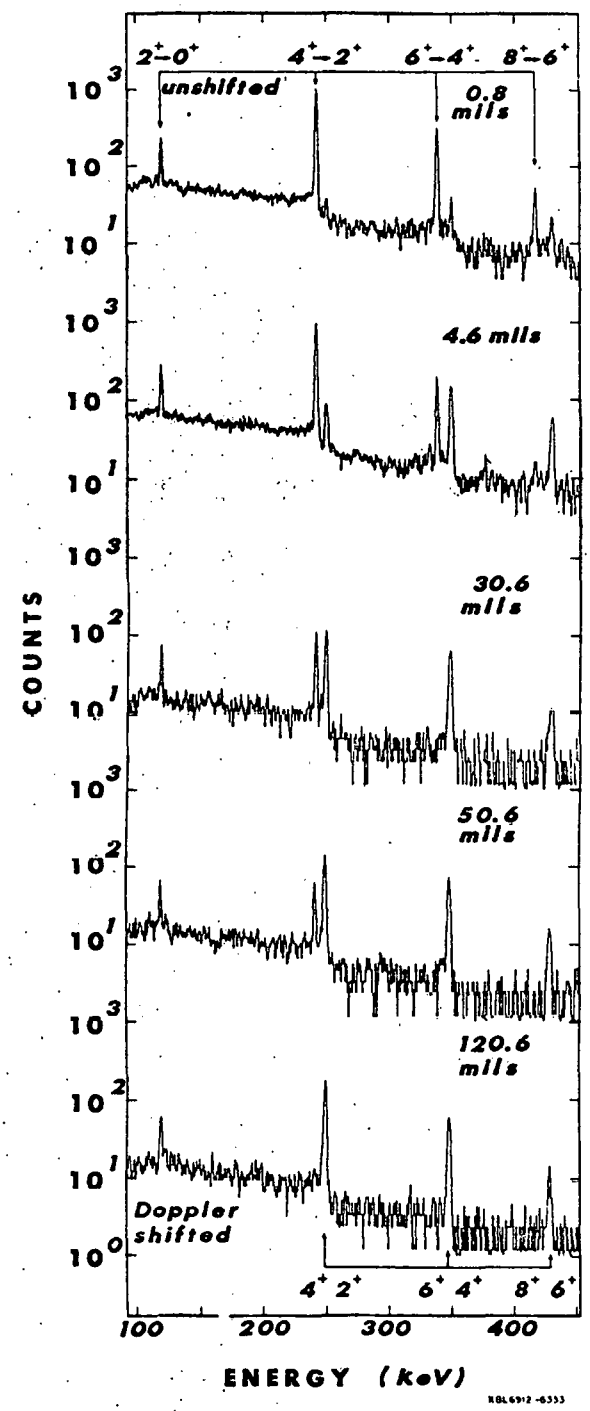
2⁺-0⁺
4⁺-2⁺
6⁺-4⁺
8⁺-6⁺
unshifted
0.8 mils
4.6 mils
30.6 mils
50.6 mils
120.6 mils
Doppler shifted
4⁺ 2⁺
6⁺ 4⁺
8⁺ 6⁺
COUNTS
ENERGY (keV)
100
200
300
400

Fig. 2

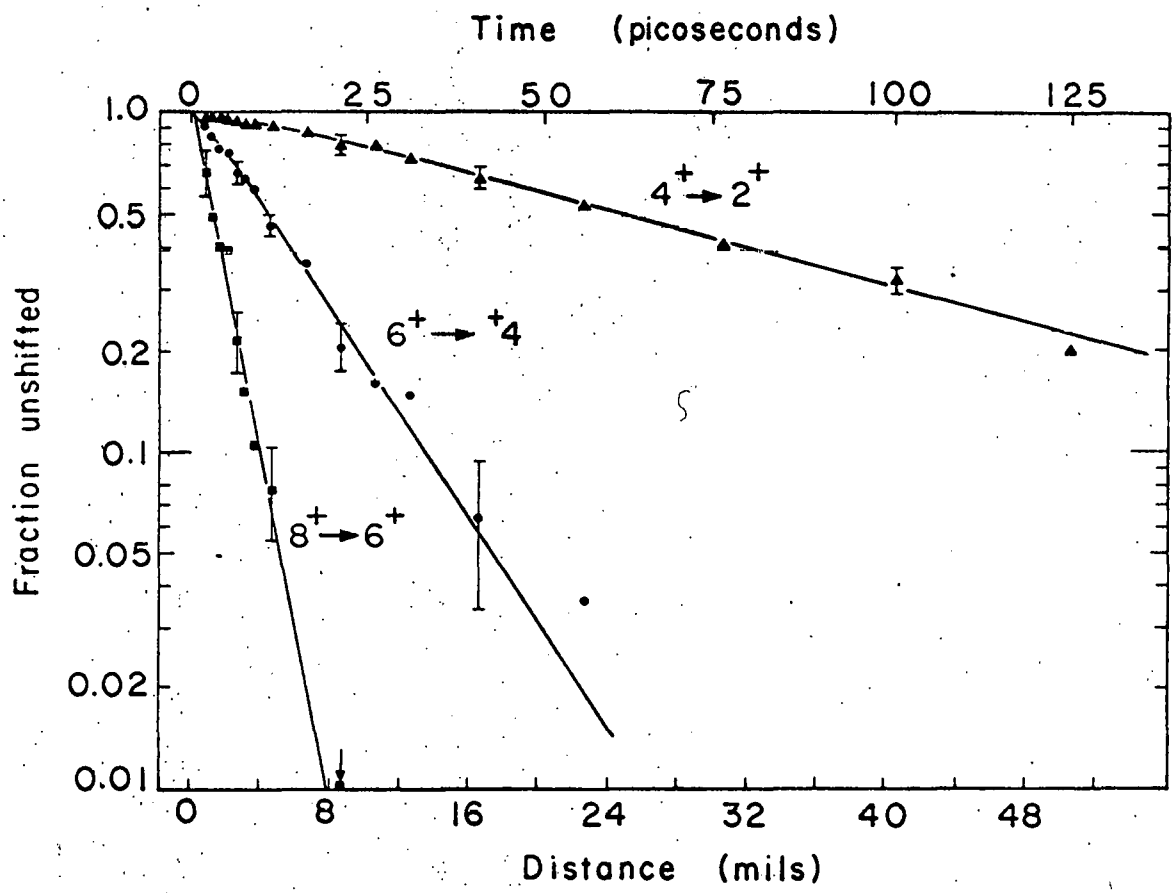

XBL695 - 2814

Fig. 3

Table I. B(E2) values for ^{152}Sm

Transition	Energy (keV)	$T_{1/2}$ (ps)	α_T	B(E2; I→I-2) exp.	rotor	D-O[b]
2 → 0	121.78	1447	1.179	0.670 ± 0.015[a]	(0.670)	(0.670)
4 → 2	244.6	58.9	0.109	0.989 ± 0.035	0.958	1.012
6 → 4	340.2	9.98	0.038	1.20 ± 0.06	1.056	1.193
8 → 6	418.7	3.10	0.021	1.39 ± 0.14	1.106	1.373

a) Average value from references 14 and 15.

b) These values have been taken from A. S. Davydov and V. I. Ovcharenko, Yadern. Fiz. 3, 1011 (1966) [translation: Soviet J. Nucl. Phys. 3, 740 (1966)] for $\mu = 0.3$, $\gamma = 10°$.

larger than the rigid rotor values based on the independently determined $B(E2; 2 \rightarrow 0)$[14,15]. If this increase is ascribed to an increase in deformation, the order of the deviations is about 1/2 - 1/3 that required to explain the deviations in the ground-band energy-level spacings. They lead, however, to values of $(\frac{\Delta\beta}{\beta})_{2^+}$ comparable to those obtained from Mössbauer[16,17] and μ-mesic X-ray studies,[18] and from mixing of the β-band into the ground band, as determined by β-band branching ratios and the values of the ground-band and inter-band B(E2)'s[19]. On the other hand, a similar study of the $8^+ \rightarrow 6^+ \rightarrow 4^+ \rightarrow 2^+ \rightarrow 0^+$ transitions in ^{154}Sm yields good agreement with the rigid rotor model[20], even though the energy-level spacings show some deviations.

The more usual determination of B(E2) and B(E3) values makes use of Coulomb excitation of the desired levels, and then comparison of the measured yields with those calculated by the deBoer-Winther program[21] using (estimated) values of all the pertinent matrix elements. The experimental yields may be obtained either from the intensity of scattered particles of the appropriate energy or from the intensity of the de-excitation gamma-rays, either in singles or in coincidence with back-scattered particles. The first method is simpler, in that one observes the direct population of the desired states without having to correct for feeding from other levels. But for heavy-ion beams the use of gamma-ray detection has the advantage of better resolution and of permitting thicker targets, and hence higher yields. I shall only discuss the latter method.

Although in some cases comparison of the experimental yields with those calculated from the computer program is a straight-forward process, in other cases it may not be. Besides accounting for the excitation of, and feeding from, a number of excited bands, and for the possible

attenuation of the initial gamma-ray angular distribution, excitation by higher moments may also have to be considered.

For example, a recent determination of the B(E2; 4 → 2) in ^{152}Sm by means of ^{4}He, ^{16}O, and ^{40}Ar Coulomb excitation yielded discordant results[19]. A partial answer to this problem appears to be inclusion of direct E4 excitation of the 4+ state. For with ^{4}He excitation this first-order process may make a significant contribution relative to the weak double E2 excitation, as may also the interference between them. Figure 4 shows the pathways considered in exciting the 4+ state, and Fig. 5 indicates the effect on the yield of that state of an E4 matrix element. To determine the size of the E4 matrix element in ^{152}Sm, the 4+ → 2+ gamma-ray yield was measured with respect to those of the 2+ → 0+ transition in ^{152}Sm and ^{150}Sm by means of Coulomb excitation with ^{4}He ions of 11.1, 10.4, and 10.0 MeV. Targets of both natural and enriched ^{152}Sm were used, and both singles and back-scatter coincidence measurements were made[22]. These two types of measurements are about equally sensitive to the E4 moment, but differ in their sensitivity to the feeding from other states. The results of the two sets of measurements agree, yielding an E4 moment of $(+0.35 \pm 0.11)eb^2$ for ^{152}Sm. (Quantal corrections will increase this slightly.) Assuming the nucleus to be rigid, axially symmetric, and uniformly charged with a sharp surface given by $R = R_0 (1 + \beta_2 Y_{20} + \beta_4 Y_{40})$, and taking the charge radius to be $1.2A^{1/3}$ F, the values $\beta_2 = 0.259$ and $\beta_4 = +0.058$ can be obtained from the measured E2 and E4 moments. These compare quite well with the values $\beta_2 = 0.246$ and $\beta_4 = 0.048$ found by Hendrie et al.[23] for the shape of the nuclear field (with the same value of R_0).

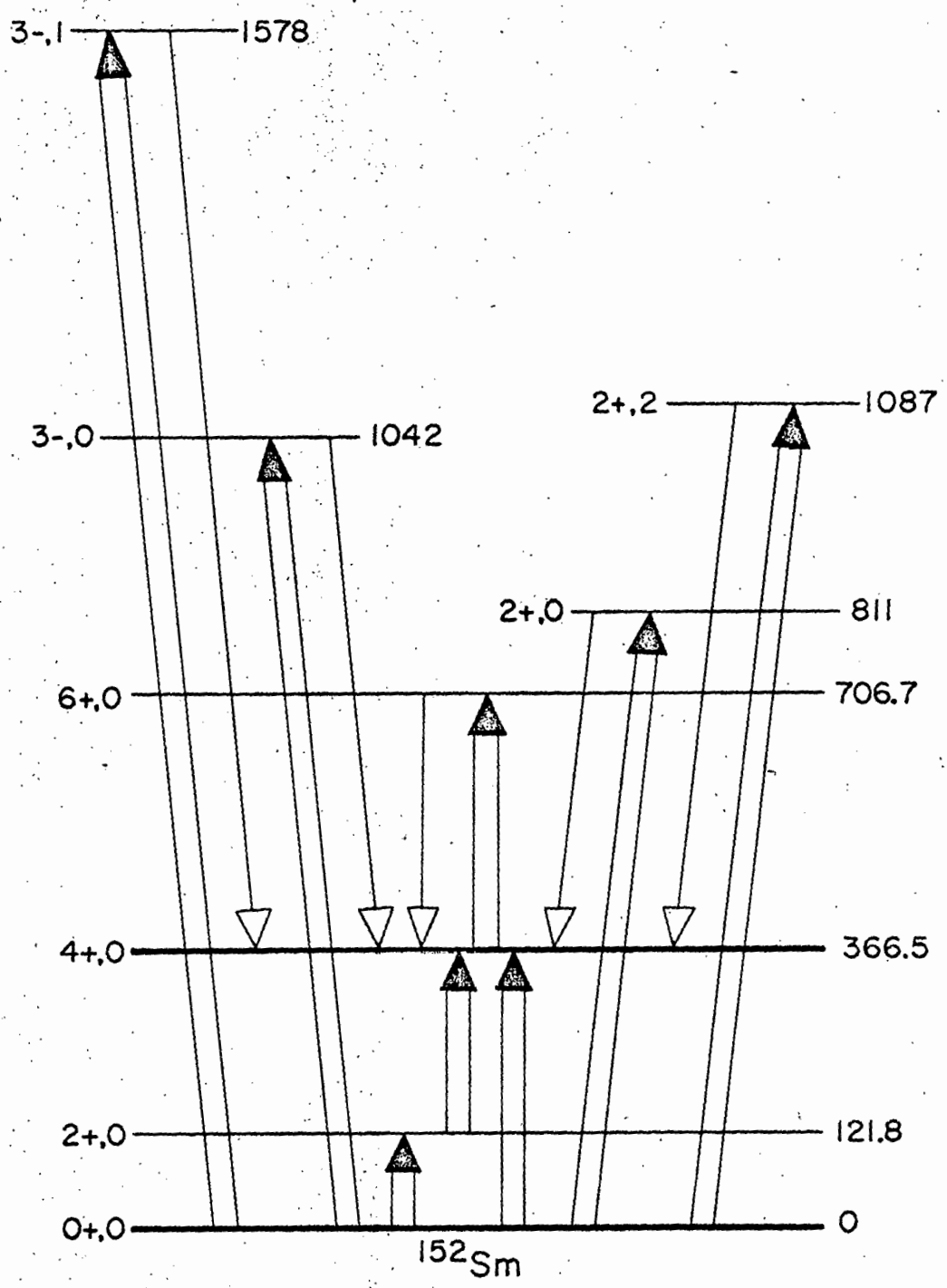

XBL708-3677

Fig. 4

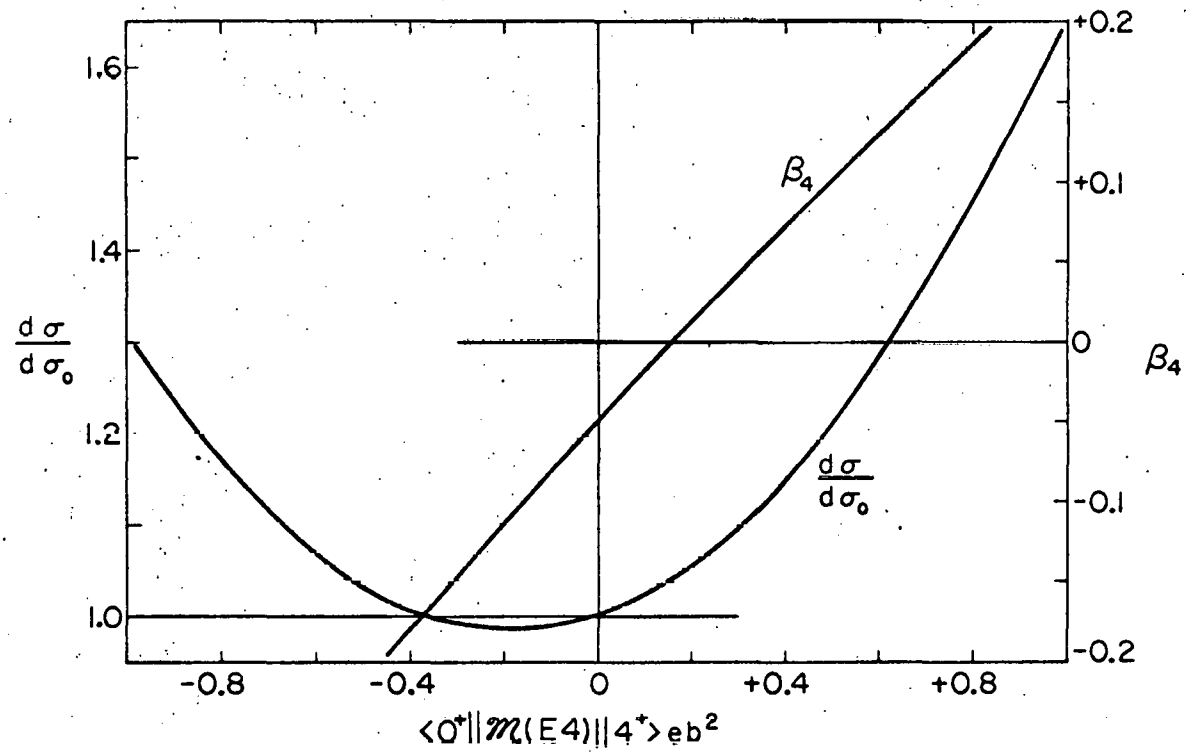

XBL703-2496

Fig. 5

Relative to the double E2 excitation, the E4 contribution to the 4+ cross section is smaller with ^{16}O excitation, and including the effect of E4 excitation, the experimental results with ^{4}He and ^{16}O excitation on ^{152}Sm are in agreement. But it should be noted the ^{40}Ar results are still in disagreement; apparently some further effect must still be found and taken into account.

Static quadrupole moments of excited states can also be measured in favorable cases by a particular type of multiple Coulomb excitation, the so-called "reorientation effect"[24]. The yield of the excited state is influenced by an interference between the direct E2 amplitude connecting the states and a double E2 amplitude involving the static moment of the excited state. The magnitude of the reorientation effect is given approximately by the ratio of the interference term to the first order term[25]; for the 2+ state of an even-even target, t,

$$r_t = \frac{A_p}{Z_t} \frac{\Delta E_t}{(1 + A_p/A_t)} \langle 2 + \| \mathcal{M}(E2) \| 2+ \rangle_t \, K(\theta,\xi) \quad , \qquad (2)$$

where A and Z are the charge and mass numbers, ΔE is the energy of the excited state, and the suffixes p and t correspond to projectile and target, respectively. The term $K(\theta,\xi)$ is a positive function which is sensitive to the particle scattering angle, θ, but not very dependent on the beam energy. The sign and magnitude of the effect depend upon the static moment; the way the experiment is usually done, namely by comparing the yields with ^{4}He and ^{16}O beams, the effect is a 5-10% change in yield of the 2+ state. The use of ^{32}S or ^{40}Ar beams doubles the effect, making a less difficult experiment, but still not an easy one. Starting with the first reorientation studies on a number of doubly-even nuclei only a half-dozen

years ago[26-31], a number of moments have been, and are being, measured. Some recent results summarized by D. Cline et al.[32] are shown in Fig. 6. Interestingly enough, almost all nuclei measured have turned out to be prolate with the exception of ^{28}Si, ^{118}Sn, and $^{194,196,198}Pt$.

A somewhat easier reorientation experiment is looking at the excitation in the projectile. In this case,

$$r_p = \frac{A_p}{Z_p} \frac{\Delta E_p}{(1 + A_p/A_t)} \langle 2 + \| \mathfrak{M}(E2) \| 2+ \rangle_p K(\theta,\xi) \quad , \qquad (3)$$

and the effect is larger than in target reorientation by Z_t/Z_p. The results of some recent doubly-even projectile reorientation measurements[36-40] in the s-d shell nuclei are shown in Fig. 7, along with a number of older odd-mass moment determinations. It is of interest to note the oscillations in the sign of the moments in the latter half of the s-d shell.

2.2. Magnetic moments

I shall only be concerned with the measurement of μ, or of $g = \mu/\mu_N I$, ($\mu_N = e\hbar/2m_p c$) for excited states, and shall consider briefly a number of variations on the perturbed angular correlation technique[41-45] that have been applied to reactions, particularly heavy-ion ones. The essence of the method is that the nuclear reaction or Coulomb excitation provides well-aligned ($m = 0$) excited nuclei, and then due to their magnetic moment these will precess under the influence of a magnetic field, causing a rotation of the gamma-ray angular distribution. Clearly, to be observed the rotation must be of the order of a few degrees, and since $\omega_L \tau = g\mu_N H\tau/\hbar$, the shorter the mean life of the state, τ, the larger must be the field, H. For lifetimes in the range of many excited states of interest, 10^{-9} - 10^{-12} sec, fields of 10^5 - 10^8 g, respectively, are needed.

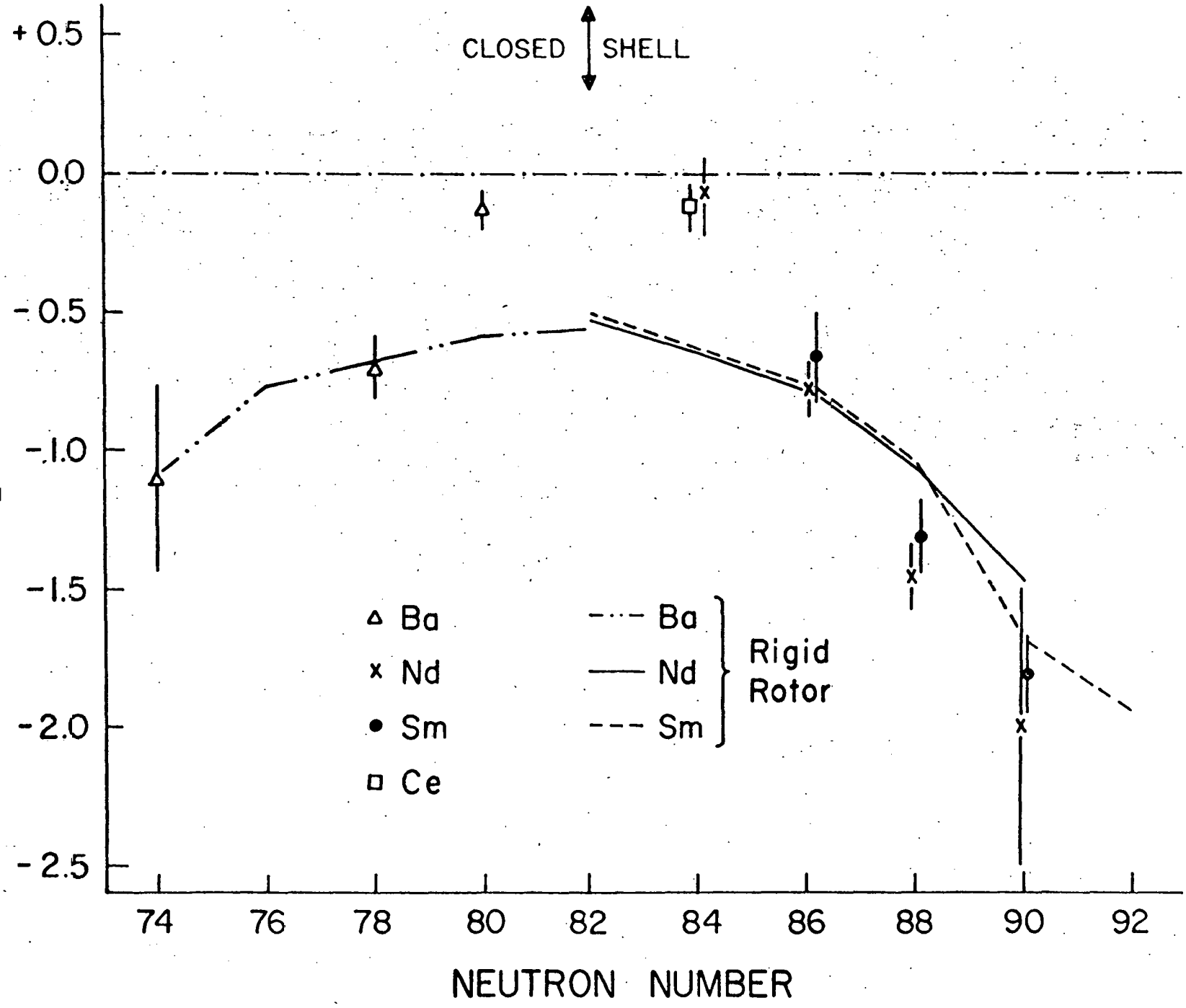
+0.5
0.0
-0.5
-1.0
-1.5
-2.0
-2.5
CLOSED SHELL
Q_{2^+} (e·b)
Ba
Nd
Sm
Ce
Ba
Nd
Sm
Rigid Rotor
74
76
78
80
82
84
86
88
90
92
NEUTRON NUMBER

Fig. 6

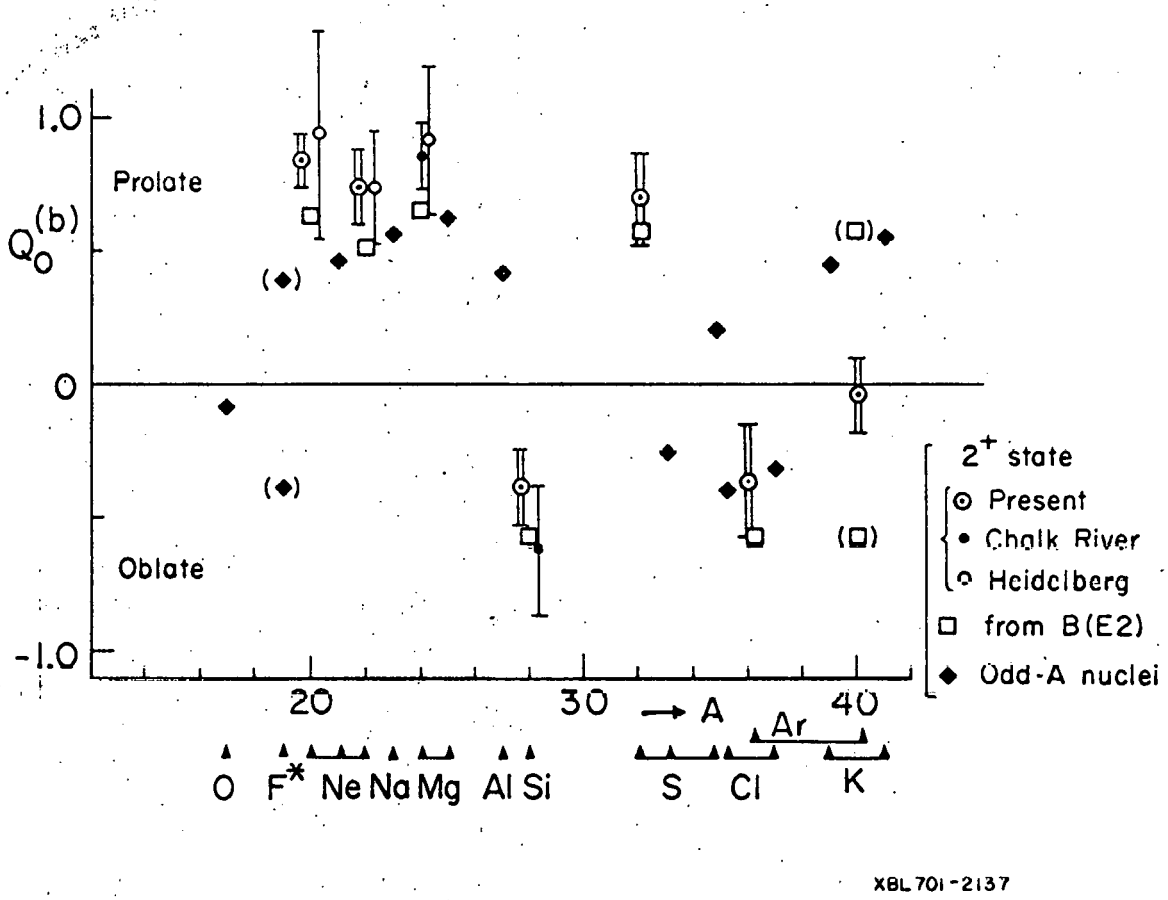
1.0
Prolate
Q_o(b)
0
Oblate
-1.0
20
30
A
40
Ar
O F* Ne Na Mg Al Si
S Cl K
2+ state
Present
Chalk River
Heidelberg
from B(E2)
Odd-A nuclei
XBL701-2137

Fig. 7

This is beyond the capabilities of present-day magnets, but two developments of the last few years using heavy-ion beams have brought this time region under attack. One, providing fields up to 50 Mg, makes use of the hyperfine field caused by the unpaired electrons of an excited ion recoiling into vacuum or gas[46,47]. Integral attenuation coefficients, $G_K = (1 + P_K \omega_L^2 \tau\tau_c)^{-1}$ (where P_K is a numerical constant and τ_c is the "atomic correlation time"), can be determined for the attenuation of the gamma-ray angular distribution with respect to unperturbed distributions measured in lead- or other-backed targets. Then if the hyperfine field (e.g., by comparison with nuclei of known g-factors) and τ_c (from recoil into gas measurements) are known, the g-factors for states as short-lived as a few picoseconds can be determined. In such an experiment, the heavy-ion reaction produces the states to be studied, aligns them, recoils them into the vacuum or gas, and causes the electronic excitation (during passage through the target) which provides the hyperfine field which attenuates the distribution.

The other method, called IMPACT, is also a time-integral PAC method[48-49]. It involves Coulomb exciting the desired state and recoiling the nucleus out of the target into a ferromagnetic foil. Requiring the de-exciting gamma-ray to be in coincidence with the back-scattered projectile that caused the excitation insures maximum linear momentum transfer and production of highly aligned (m = 0) nuclei, so that usually a strongly anisotropic gamma-ray distribution results. Internal fields of 10^6 g are obtainable in this fashion, so that many states with $\tau \sim 0.1$ nsec (particularly the first excited 2+ in vibrational nuclei) have been studied this way. But a discrepancy has always been found between the precession angle (or internal field) with IMPACT measurements and that with time-

integral PAC using radioactive sources melted or implanted into the ferromagnetic material[50]. This is now known to arise from a short-lived (psec) field acting on the recoiling nucleus in the former case[50,51]. However, this process does not disturb the determination of g-factors if the effective reduction in the internal field is taken into account. This method can be used for nuclei with $\tau \leqslant 10^{-9}$ sec. A somewhat similar technique, but allowing the excited nucleus to recoil into a suitable environment (which does not perturb the alignment) placed in an external magnetic field[52-54], permits measurements from 10^{-9} sec on down to 10^{-6} sec.

But an exciting step in magnetic moment studies has been the development of time-differential PAD methods involving nuclear reactions with pulsed beams, that is, the study of isomers in the range 10^{-8} - 10^{-3} sec[55-59]. Again the reaction itself produces the nuclear alignment and the linear momentum to recoil the product into a suitable environment (cubic crystal, liquid or molten target) where other perturbations are a minimum. By choosing the target-projectile system properly, a variety of isomers can be made and studied. The fact that this is a singles measurement permits reasonable statistics in a time-differential method. And since only the isomeric (out-of-beam) transitions are of interest, a very clean spectrum usually results. Figure 8 shows the out-of-beam spectrum we have observed[60] from the 123 μsec 7- state in ^{206}Pb made by the reaction ^{204}Hg(^{4}He, 2n)^{206}Pb with a pulsed beam from the HILAC. The liquid mercury target itself provides the stopping environment, and is placed between the poles of an electromagnet. As the gamma-ray angular distribution from the aligned isomers rotates in the field, the intensity recorded by one, or more, gamma detectors oscillates with (twice) the Larmor frequency and decays with the mean life of the state. By taking the appropriate ratio of gamma-ray yields,

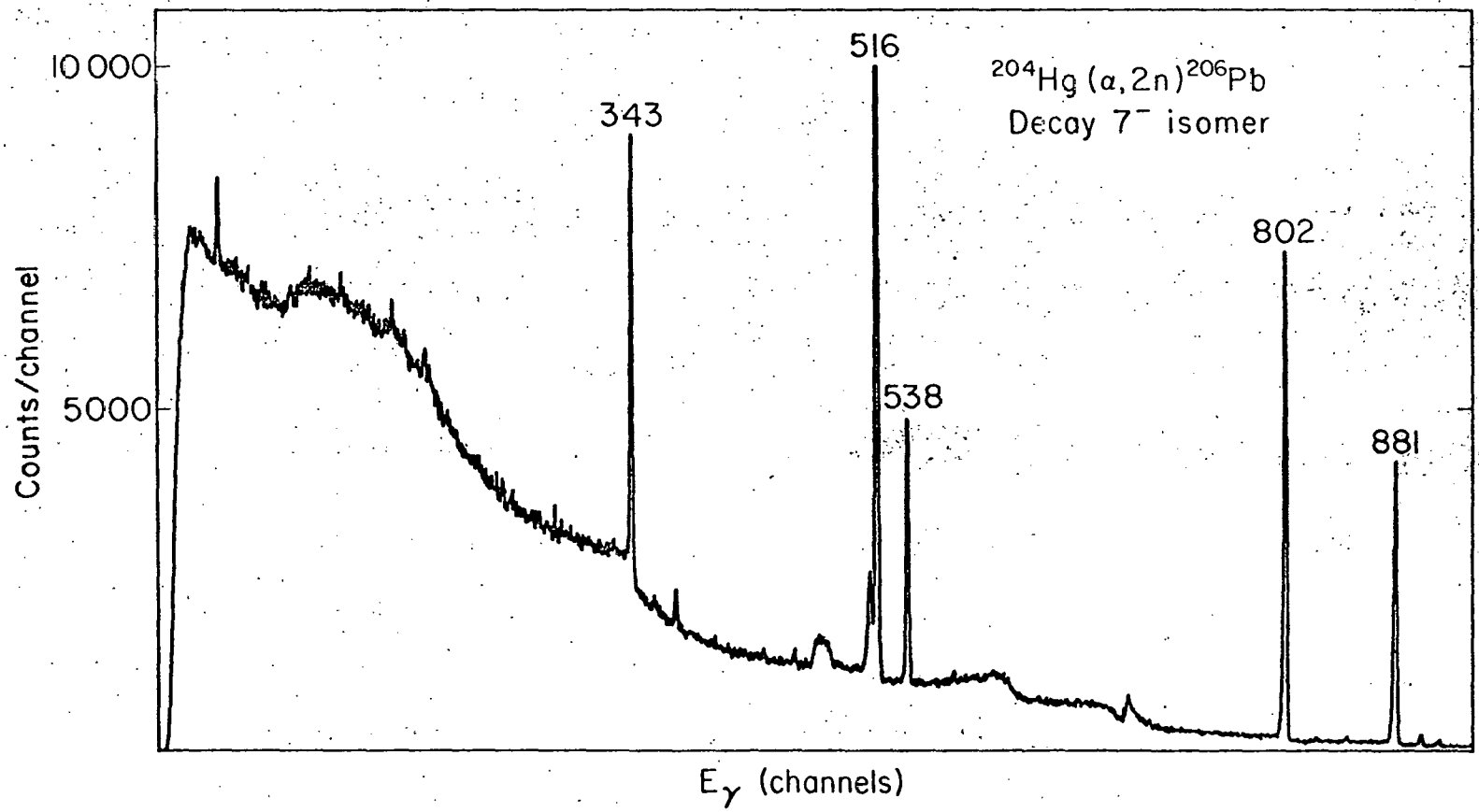

Fig. 8

XBL705-2875

involving field up and field down for one detector, or involving two detectors at appropriate angles to the beam direction, the decay factor cancels out leaving a simple oscillation. This is shown in Fig. 9 for the 516 keV transition from the ^{206}Pb isomer for the case of two detectors, one at 20° and the other at -70° to the beam.

An ingenious variation of this technique for isomers with $\tau > T$, the beam repetition time, has been developed by Christiansen et al.[61], the "stroboscopic method." In this, the Larmor frequency is brought into resonance with the beam repetition rate or its harmonic $T = n\pi/\omega_L$ with $n = 1,2,3...$, by carefully varying the external magnetic field. Thus the transitions from the isomeric states formed in different beam pulses add coherently. We have also applied this technique to the g-factor measurement of the 7- state in ^{206}Pb (Ref. 60). Two Ge(Li) detectors are placed at ± 45° to the beam direction and each provides two out-of-beam spectra; one taken during a time interval centered at 1/4 the beam repetition interval and the other at 3T/4. Figure 10 shows the double ratio for the 516 keV transition

$$\frac{Y\,(T/4,\ 45°)}{Y\,(3T/4,\ 45°)} \Big/ \frac{Y(T/4,\ -45°)}{Y(3T/4,\ -45°)}$$

vs the field, H. This and the previous method agree on a value of the g-factor for the 7- state in ^{206}Pb of -0.0217 ± 0.0004.

These techniques, as well as the use of NMR with the longer-lived isomers[62-63], will surely be more commonly employed in the future and will contribute greatly to our knowledge of hyperfine interactions and nuclear magnetic moments.

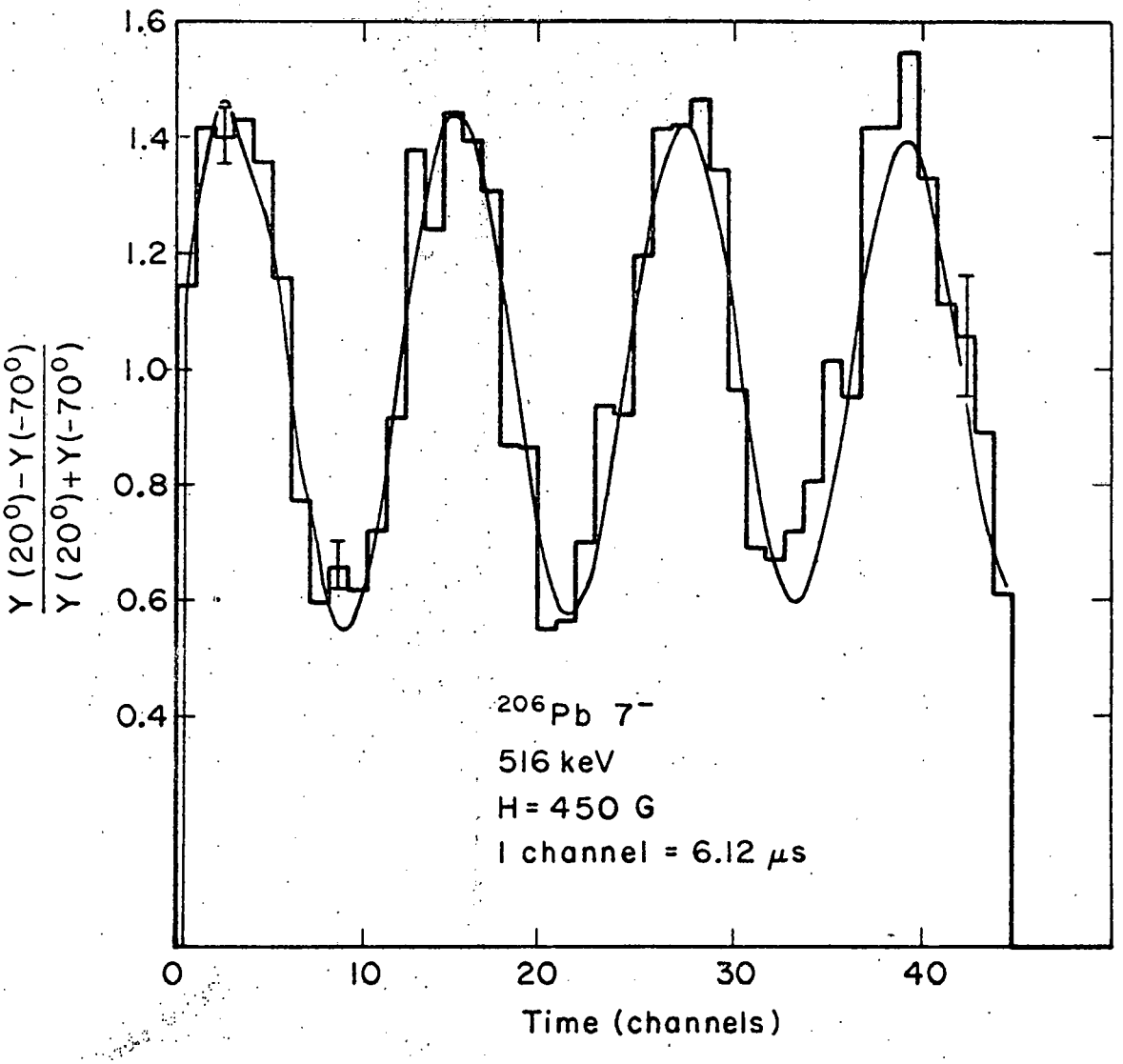

XBL705-2873

Fig. 9

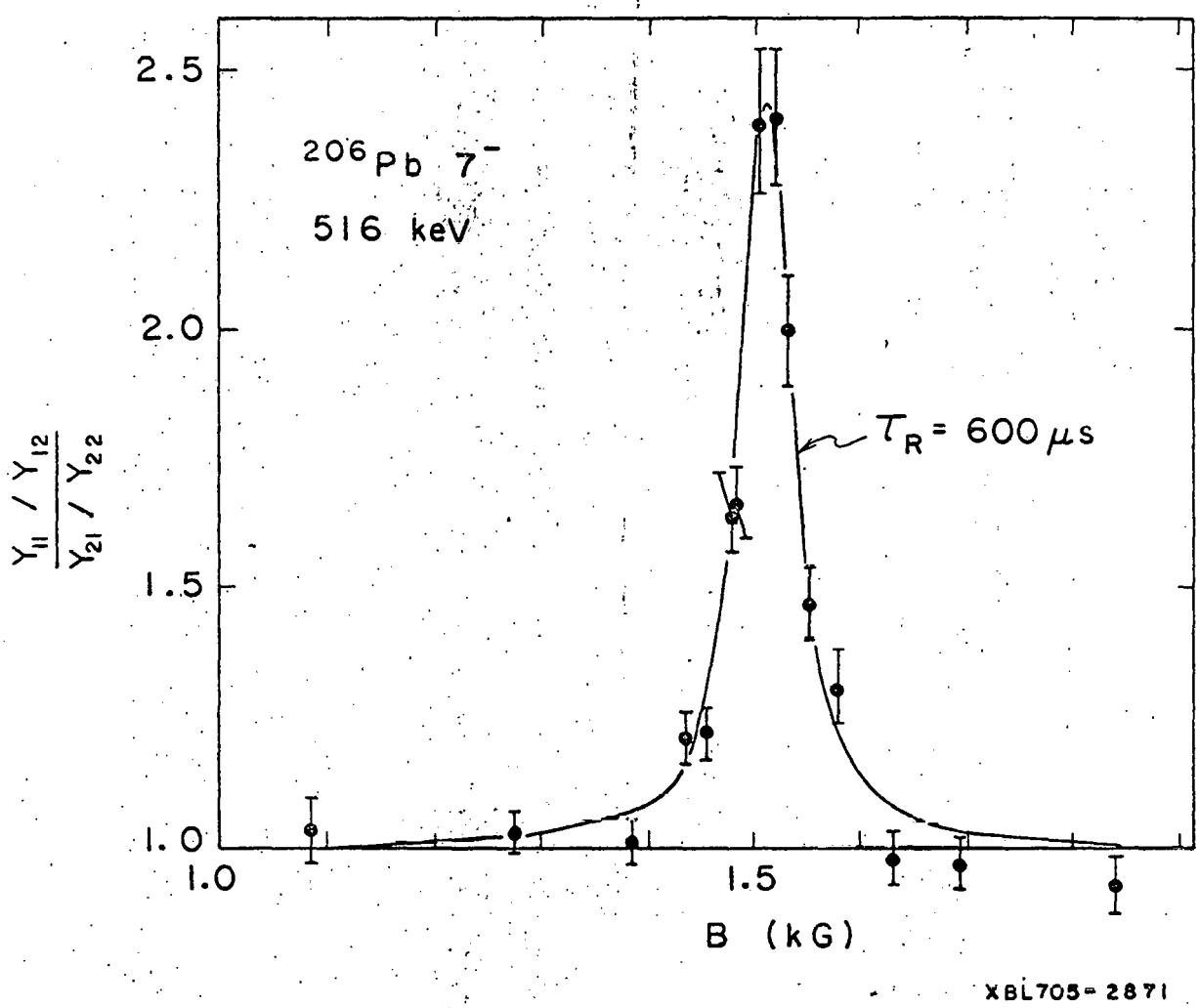
^{206}Pb 7$^-$
516 keV
τ_R = 600 μs
$\frac{Y_{11} / Y_{12}}{Y_{21} / Y_{22}}$
2.5
2.0
1.5
1.0
1.0
1.5
B (kG)
XBL705-2871

Fig. 10

3. ENERGY LEVELS SYSTEMATICS

One of the first principal uses of in-beam spectroscopy was to make a systematic study of the energy levels of a wide range of neutron-deficient nuclei, particularly of the even-even species[64-67]. By using the lowest (H.I., xn) reaction of reasonable yield above the Coulomb barrier, one obtains rather clean spectra. And because large amounts of angular momentum are brought into the product nucleus, the decay is from high-spin states down to the ground state; first a rapid passage ($\leq$ 10 picoseconds)[11] through the yrast bands[68-69], and then where they cross the ground-state band (just above the pairing gap) a transfer into the latter. Thus, with even-even nuclei the ground-state rotational band, or the highest-spin member of each multiplet in a vibrational band, is usually seen with most of the intensity of the cross section for that nucleus. An enormous amount of data on such quasi-rotational ground bands has come out from a number of laboratories, so that there is not space here to summarize it all. I shall only touch briefly on a few topics.

An illustrative and interesting sequence of such quasi-rotational bands is shown in Fig. 11 for the doubly-even cerium nuclei extending from mass 126 to 150. The neutron-deficient ceriums were made by Sn(^{16}O, xn)Ce reactions[70] and the data on the neutron-excess ones were obtained by Wilhelmy *et al.*[71] by "in-beam" studies on the spontaneous fission of ^{252}Cf. At each end of the mass scale a region of deformed nuclei appears to be entered, and in the center there is a change in the energy level scheme for the singly-magic ^{140}Ce.

One important characteristic to note from the energy-level systematics that has appeared from mass 80 on up is that, with few exceptions, the levels of a given spin, or the ratio of the level energies, change quite

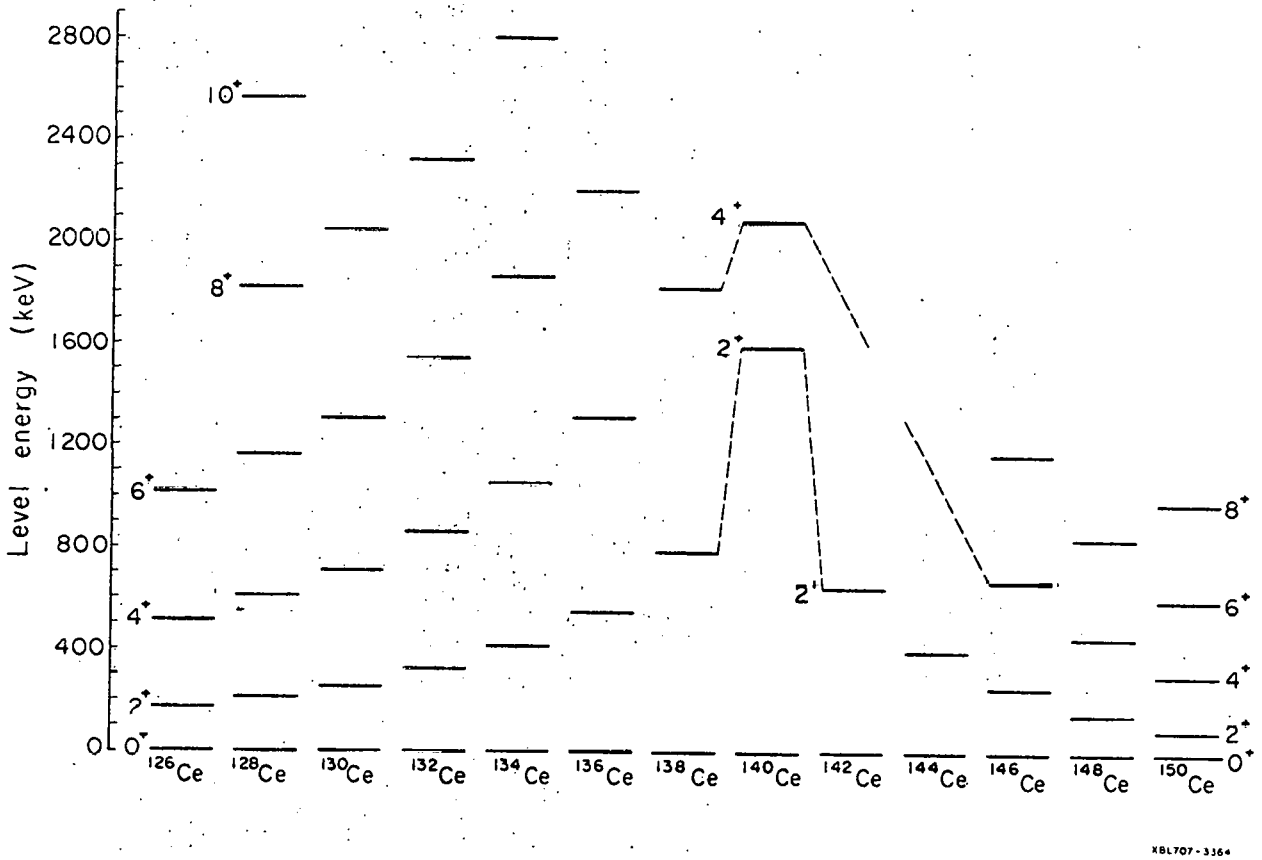
Level energy (keV)
2800
2400
2000
1600
1200
800
400
0
10+
8+
6+
4+
2+
0+
4+
2+
2+
8+
6+
4+
2+
0+
126Ce
128Ce
130Ce
132Ce
134Ce
136Ce
138Ce
140Ce
142Ce
144Ce
146Ce
148Ce
150Ce
XBL707-3364

Fig. 11

smoothly as neutrons or protons are added. There are two types of exceptions. One occurs at magic-number nuclei where the dominance of the short-range component in the residual interaction between pairs of nucleons depress the 0^+ ground state greatly, and only slightly spread the 2^+, 4^+, ... states of the $(j)^2$ broken-pair configuration. This was already shown in Fig. 11 for ^{140}Ce, and also occurs for the other 82-neutron nuclei, ^{142}Nd and ^{144}Sm, and for the 50-neutron nuclei ^{92}Mo and ^{94}Ru, Fig. 12 (Ref. 72). The other type of exception may occur when one type of nucleon has approximately half-filled a shell and the number of the other type increases from or decreases to 6 or 8 particles from a closed shell. This is shown in Fig. 13 where the ratio of the energies of the 4+ to 2+ states are shown vs proton number for various curves representing neutron number; the well known discontinuity between 88 and 90 neutrons shows up[73], but only when Z is midway between 50 and 82 protons. As the proton magic number is approached the nuclei become too stiff to deform suddenly and the ratios should turn down towards two. This is perhaps better shown in Fig. 14 which illustrates the complementary situation where the nuclei are approaching the proton shell closure at 82 rather than leaving the neutron shell at 82. There is no break as neutrons are added to osmium for example, but there is a jump in the 4+/2+ ratio between 76 and 78 protons when the neutron number is midway between 82 and 126. For nuclei near these (magic) numbers of neutrons, the ratios decrease toward two leaving little gap between 76 and 78 protons.

A second characteristic feature that should be mentioned is that, with the exception of magic-number nuclei, transition energies in the quasi-rotational bands of the doubly-even nuclei appear to become more similar as the angular momentum increases. This behavior is probably related to the

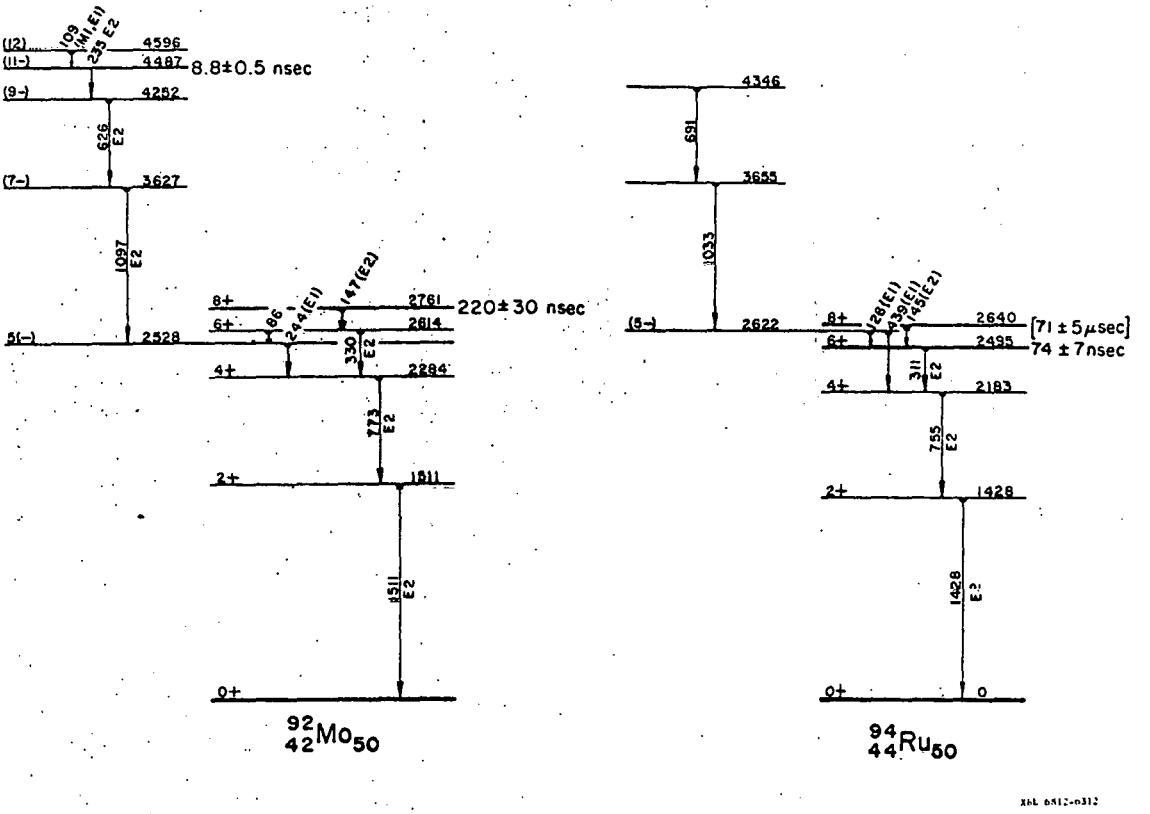
(12)
(11-)
(9-)
(7-)
5(-)
8+
6+
4+
2+
0+
4596
4487
4252
3627
2528
2761
2614
2284
1811
0
109 (M1,E1)
235 E2
626 E2
1097 E2
147(E2)
86
244(E1)
330 E2
773 E2
1511 E2
8.8±0.5 nsec
220±30 nsec
92 42 Mo 50
4346
3655
2622
691
1033
8+
6+
4+
2+
0+
2640
2495
2183
1428
0
128(E1)
439(E1)
145(E2)
311 E2
755 E2
1428 E2
[71 ± 5 μsec]
74 ± 7 nsec
94 44 Ru 50

Fig. 12

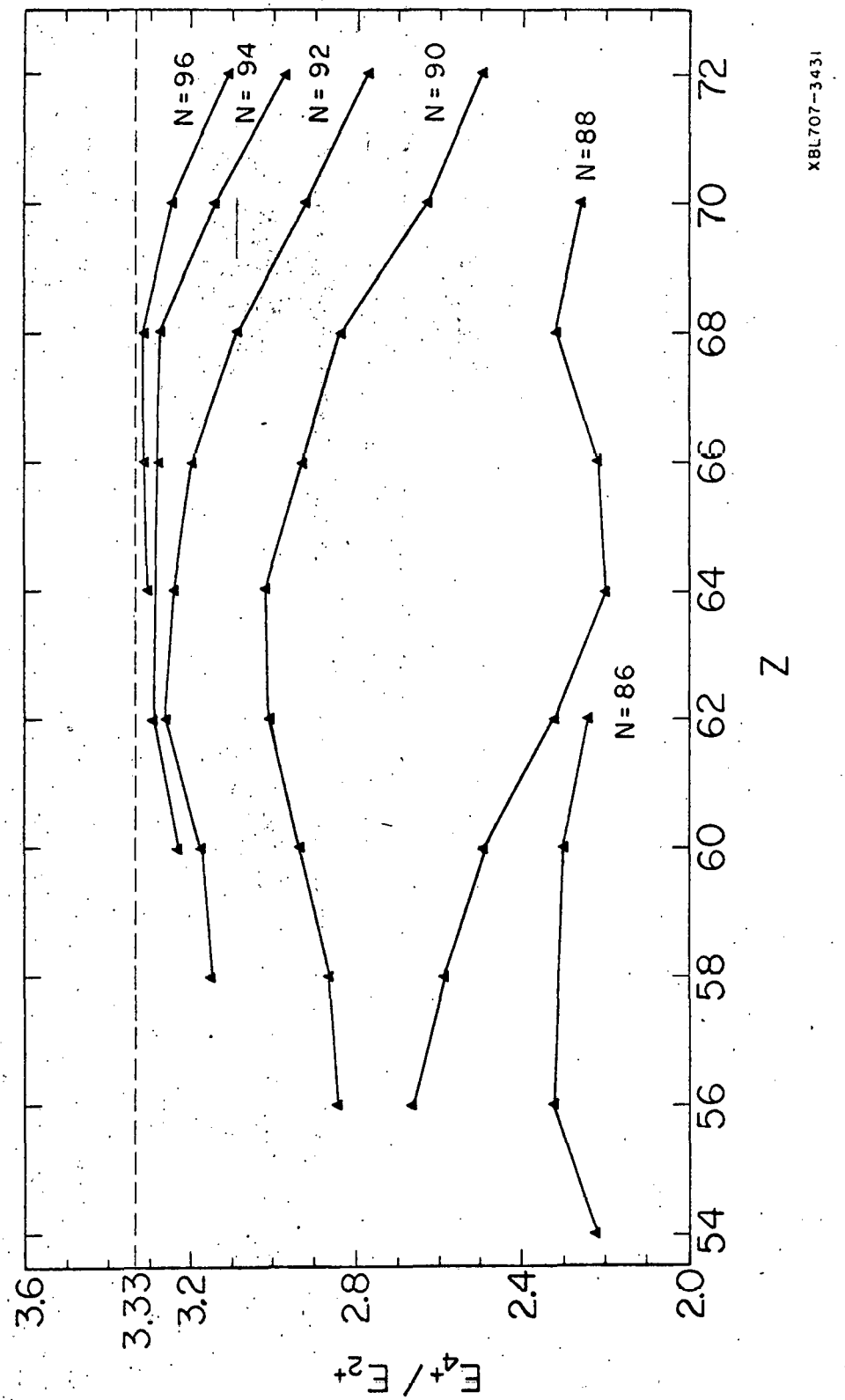
N=96
N=94
N=92
N=90
N=88
N=86
3.6
3.33
3.2
2.8
2.4
2.0
54
56
58
60
62
64
66
68
70
72
Z
E_{4^+} / E_{2^+}
XBL707-3431

Fig. 13

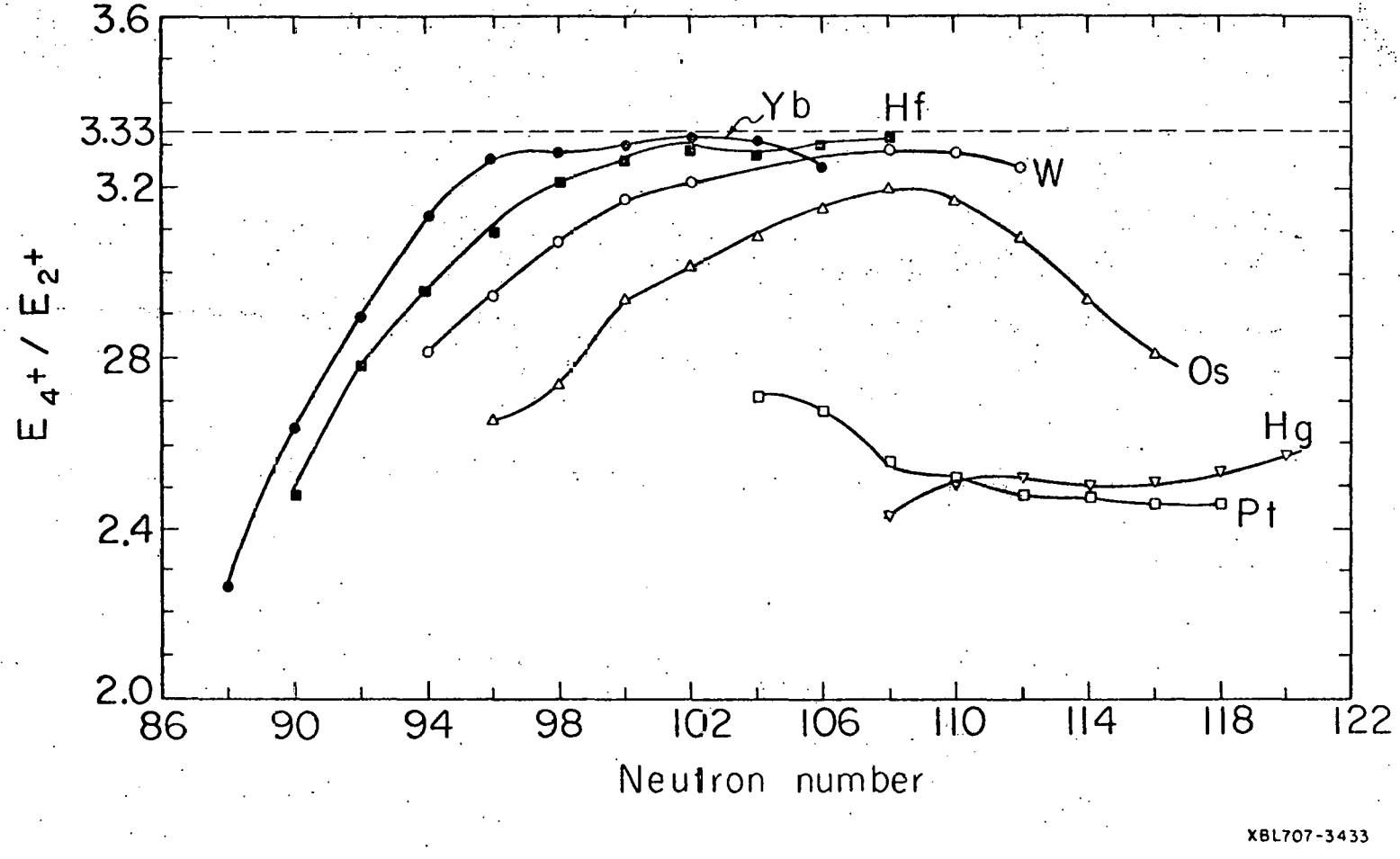
3.6
3.33
3.2
2.8
2.4
2.0
E_{4^+} / E_{2^+}
Yb
Hf
W
Os
Hg
Pt
86
90
94
98
102
106
110
114
118
122
Neutron number
XBL707-3433

Fig. 14

deviations from rigid-rotor behavior in the deformed nuclei, and is not well understood, as yet. That is, the nuclei may stretch under rotation (mixing with the β-band and γ-band), lose their pairing (mixing with the pairing vibrational band), and, in fact, the high-spin members, may mix with a great number of higher-lying states. This mixing with a large number of states may provide the statistical smoothing of transition energies which seem to be observed for many (but not all) even-even nuclei studied.

With odd-mass nuclei, the ground-state band is not uniquely depressed by the pairing energy, and so a number of bands may co-exist at low energies. Because of the large amount of angular momentum brought in by heavy-ion projectiles, the reaction will usually pick out the bands of highest intrinsic spin, and not necessarily the ground band[74]. The most important type of mixing in odd-mass deformed nuclei is caused by Coriolis coupling between bands differing in K by ± 1; it is most pronounced for those bands that have come down from the oscillator shell above, the unique parity bands in a shell, as these are derived from high j states and can mix readily only with their own members. The first-order effect of this mixing is to increase the effective moment of inertia in the expression for the energy[75,76]

$$E_I = E_0 + AI(I+1) + BI^2(I+1)^2 \qquad K \neq 1/2 \quad , \qquad (4)$$

where $A = \hbar^2/2\mathfrak{J}$. Stronger coupling causes the usually negative B-term to go positive, and introduces an oscillation in the energy level spacings by a higher-order Coriolis coupling to the K = 1/2 member of the system. This sequence of behavior is well shown by the odd-mass Ho nuclei whose ground-band energy level schemes are shown in Fig. 15 (Ref. 77). The ground band is based on the $7/2^-$ [523] Nilsson level derived from the $h_{11/2}$ shell-model orbit, and so is an example of the unique parity bands in a shell. The

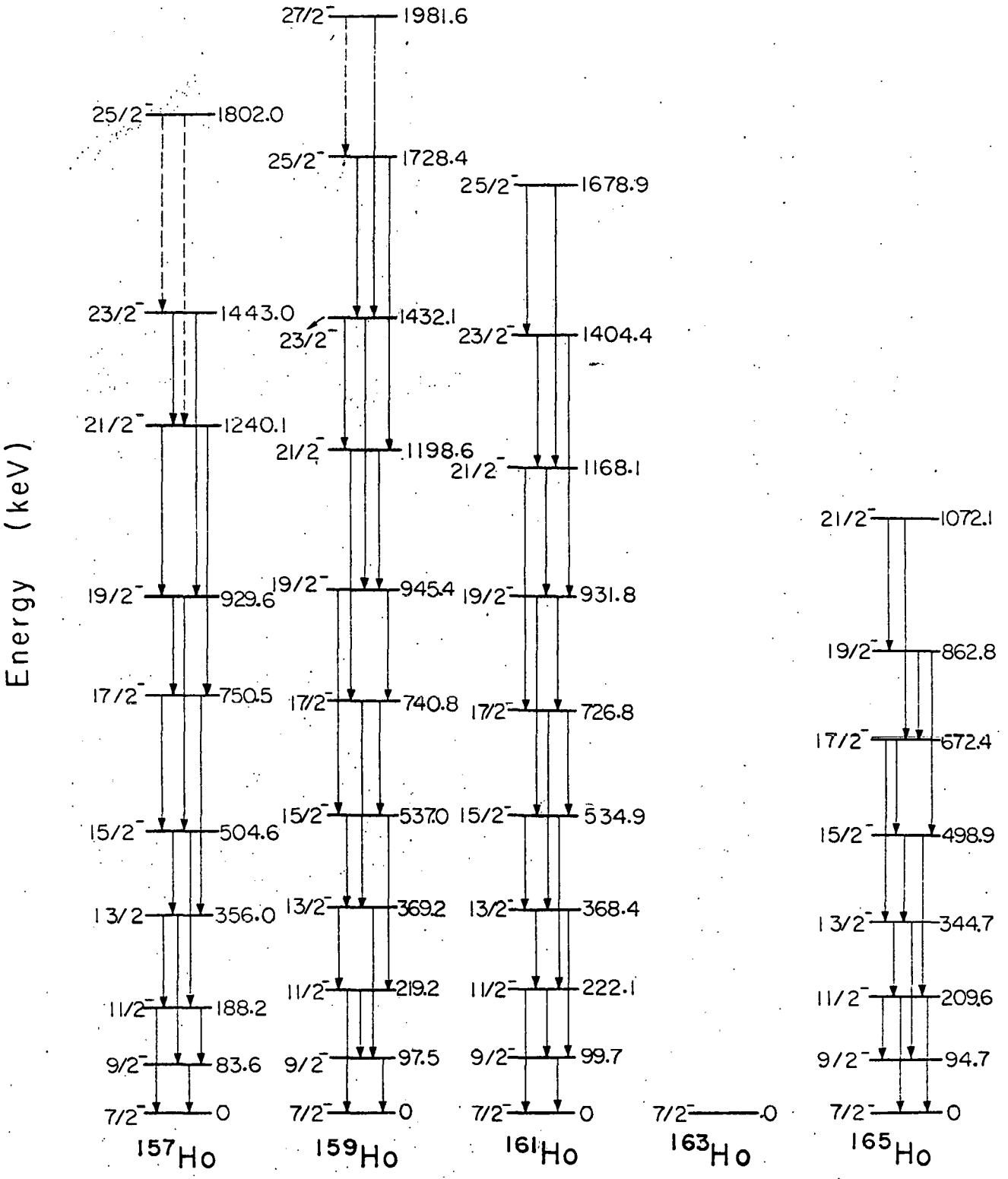
Energy (keV)
27/2⁻ 1981.6
25/2⁻ 1802.0
25/2⁻ 1728.4
25/2⁻ 1678.9
23/2⁻ 1443.0
23/2⁻ 1432.1
23/2⁻ 1404.4
21/2⁻ 1240.1
21/2⁻ 1198.6
21/2⁻ 1168.1
21/2⁻ 1072.1
19/2⁻ 929.6
19/2⁻ 945.4
19/2⁻ 931.8
19/2⁻ 862.8
17/2⁻ 750.5
17/2⁻ 740.8
17/2⁻ 726.8
17/2⁻ 672.4
15/2⁻ 504.6
15/2⁻ 537.0
15/2⁻ 534.9
15/2⁻ 498.9
13/2 356.0
13/2⁻ 369.2
13/2⁻ 368.4
13/2⁻ 344.7
11/2⁻ 188.2
11/2⁻ 219.2
11/2⁻ 222.1
11/2⁻ 209.6
9/2⁻ 83.6
9/2⁻ 97.5
9/2⁻ 99.7
9/2⁻ 94.7
7/2⁻ 0
7/2⁻ 0
7/2⁻ 0
7/2⁻ 0
7/2⁻ 0
157Ho
159Ho
161Ho
163Ho
165Ho
XBL707-3362

Fig. 15

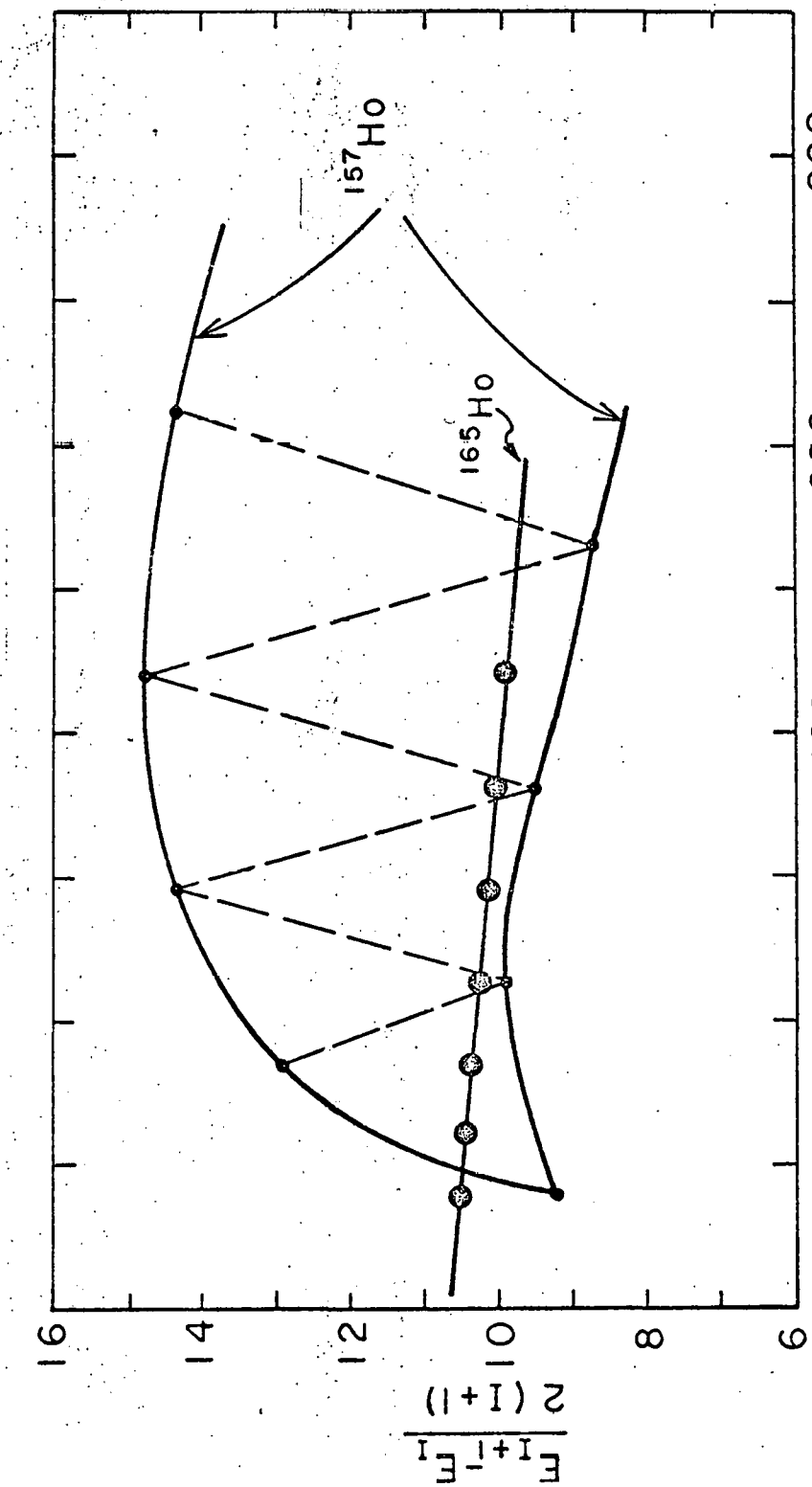
^{157}Ho
^{165}Ho
16
14
12
10
8
6
200
400
600
800
$\frac{E_{I+1}-E_I}{2(I+1)}$
$4(I+1)^2$
XBL707-3366

Fig. 16

levels in ^{165}Ho follow Eq. (4) rather well, with A = 10.65 and B = -3.2×10^{-3}. The values of A and B are slightly smaller than for the neighboring even-even nuclei, as expected. For these latter nuclei, the spacings go up as neutrons are removed and the deformed region is left. But as can be seen in Fig. 15, the average spacing in ^{161}Ho, ^{159}Ho, and ^{157}Ho stays about the same; this is the compression of the band or increase in effective moment of inertia mentioned above. As the nuclei move towards lower deformation, the h 11/2-derived bands come closer together, the Coriolis coupling becomes stronger, and one can also see the oscillation in the energy level spacings develop. Figure 16 shows this in a plot of $(E_{I+1} - E_I)/2(I+1)$ vs $4(I+1)^2$ for ^{165}Ho and ^{157}Ho; the slope of such a plot gives B/2 in Eq. (4) and the intercept yields A. The values for ^{165}Ho are as already mentioned, but for ^{157}Ho it is hard to say more than that B is positive, the effective moment of inertia is about the rigid value, and that the oscillations are very large. A perturbation expression such as Eq. (4) is inadequate, and a complete Coriolis coupling calculation involving all the other bands from the h 11/2 orbits is required. Such a calculation does yield a reasonable value of the moment of inertia for all the bands involved.

Hjorth et al.[78] have discussed a similar situation for the odd-mass ^{161,163,165}Er where the Coriolis coupling is between members of the i 13/2 neutron orbits, and in particular the 1/2+[660] to 7/2+[633] bands. The resulting mixed band is not the ground band, but because of its large moment of inertia, its levels are among the lowest-lying of a given (high) spin, and so the sequences shown in Fig. 17 get most of the reaction intensity. We have also observed ^{159,157}Er (Ref. 79), and it can be seen that these nuclei show the same trend. The oscillations in the energy level spacings have become large enough by ^{161}Er to invert the spin order of each pair of

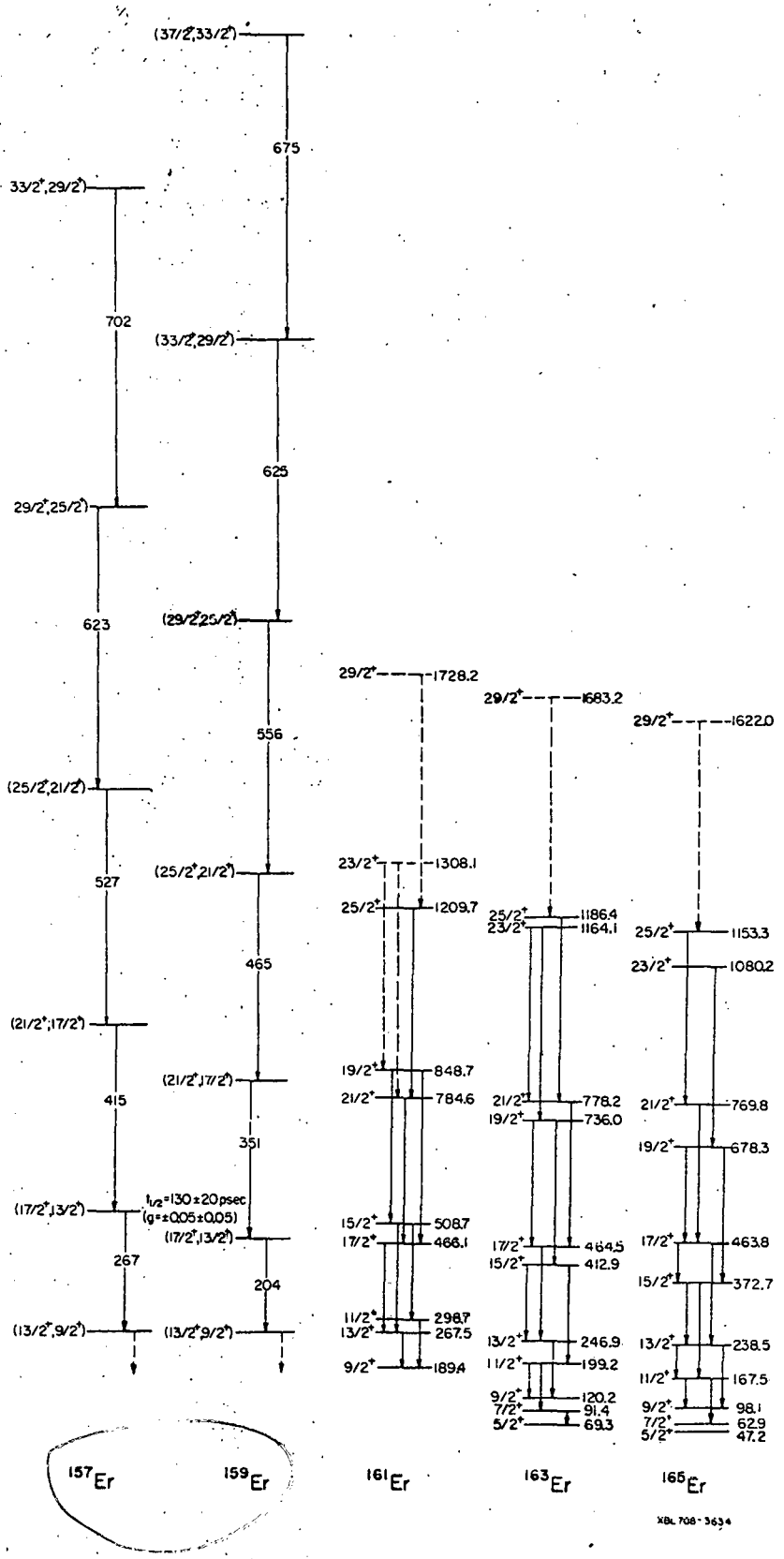
(37/2⁺,33/2⁺)
675
33/2⁺,29/2⁺
702
(33/2⁺,29/2⁺)
625
29/2⁺,25/2⁺
623
(29/2⁺,25/2⁺)
556
(25/2⁺,21/2⁺)
527
(25/2⁺,21/2⁺)
465
(21/2⁺,17/2⁺)
415
(21/2⁺,17/2⁺)
351
(17/2⁺,13/2⁺)
t1/2=130±20psec
(g=±0.05±0.05)
(17/2⁺,13/2⁺)
267
204
(13/2⁺,9/2⁺)
(13/2⁺,9/2⁺)
157Er
159Er
29/2⁺ 1728.2
23/2⁺ 1308.1
25/2⁺ 1209.7
19/2⁺ 848.7
21/2⁺ 784.6
15/2⁺ 508.7
17/2⁺ 466.1
11/2⁺ 298.7
13/2⁺ 267.5
9/2⁺ 189.4
161Er
29/2⁺ 1683.2
25/2⁺ 1186.4
23/2⁺ 1164.1
21/2⁺ 778.2
19/2⁺ 736.0
17/2⁺ 464.5
15/2⁺ 412.9
13/2⁺ 246.9
11/2⁺ 199.2
9/2⁺ 120.2
7/2⁺ 91.4
5/2⁺ 69.3
163Er
29/2⁺ 1622.0
25/2⁺ 1153.3
23/2⁺ 1080.2
21/2⁺ 769.8
19/2⁺ 678.3
17/2⁺ 463.8
15/2⁺ 372.7
13/2⁺ 238.5
11/2⁺ 167.5
9/2⁺ 98.1
7/2⁺ 62.9
5/2⁺ 47.2
165Er
XBL 708-3634

Fig. 17

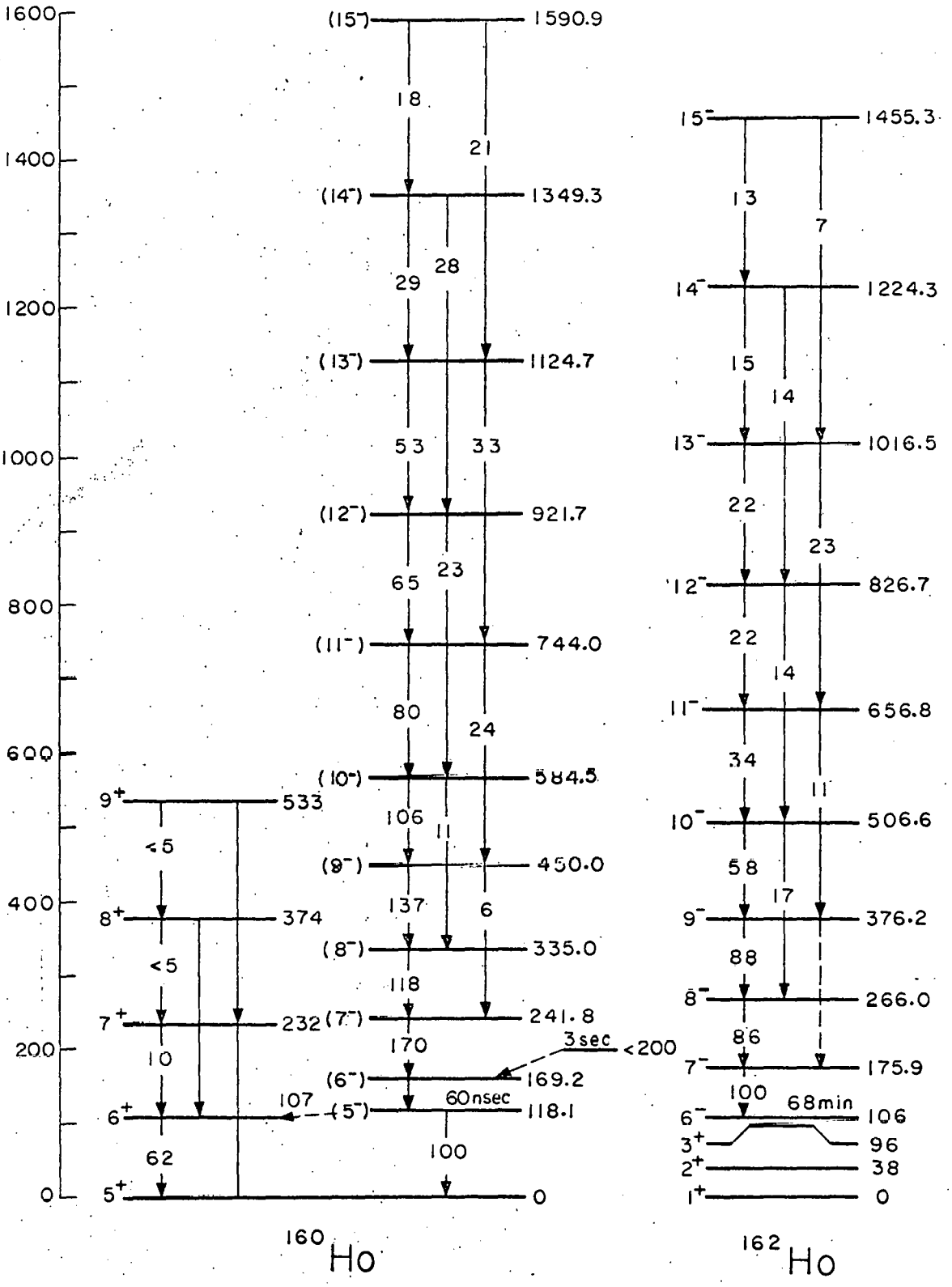
1600
1400
1200
1000
800
600
400
200
0
(15⁻) 1590.9
18
21
(14⁻) 1349.3
29
28
(13⁻) 1124.7
53
33
(12⁻) 921.7
65
23
(11⁻) 744.0
80
24
(10⁻) 584.5
106
11
(9⁻) 450.0
137
6
(8⁻) 335.0
118
(7⁻) 241.8
170
3sec <200
(6⁻) 169.2
107
60nsec
(5⁻) 118.1
100
9⁺ 533
<5
8⁺ 374
<5
7⁺ 232
10
6⁺
62
5⁺ 0
160 Ho
15⁻ 1455.3
13
7
14⁻ 1224.3
15
14
13⁻ 1016.5
22
23
12⁻ 826.7
22
14
11⁻ 656.8
34
11
10⁻ 506.6
58
17
9⁻ 376.2
88
8⁻ 266.0
86
7⁻ 175.9
100
68min
6⁻ 106
3⁺ 96
2⁺ 38
1⁺ 0
162 Ho
XBL707-3363

Fig. 18

levels. Again a complete calculation including the mixing of all the i 13/2 bands gives agreement with experiment.

Both of the series of odd-mass nuclei mentioned above show large Coriolis couplings. If the Er odd-neutron and Ho odd-proton are combined, as in the odd-odd ^{160,162}Ho, we might expect still smaller energy level spacings for this band. These bands are shown in Fig. 18, and, indeed, do have very large moments of inertia[80]. In beta-decay from the ground (not isomeric) state of a doubly-even nuclei, usually no, or few, gamma-ray transitions are observed in the odd-odd daughter nucleus. But with the proper choice of target-projectile system, cascade decay from high-spin states in a number of odd-odd nuclei, can and will be studied in- and out-of-beam in the future.

4. HOW NEUTRON DEFICIENT CAN WE GET?

The limitation on how neutron deficient we can get in (H.I.,xn) reactions comes from the onset of charged-particle evaporation, and for the heavier nuclei, from fission. We shall consider explicitly only proton and alpha emission, and so will limit ourselves to the region below Pb in the Periodic Table. After production of the compound nucleus, each step in the evaporation cascade is a competition between neutron emission and the loss of a proton or alpha (the latter events prevent formation of a more neutron-deficient product). This can be represented by

$$\sigma(xn) = \sigma_c \prod_{i=1}^{x} \frac{\Gamma_{ni}}{\Gamma_i} \quad , \tag{5}$$

where $\Gamma_i = \sum_\beta \Gamma_{\beta_i}$ and β can be n, p, or α. Also, we take

$$\frac{\Gamma_\beta}{\Gamma} = N \exp\left[-\frac{B^*_\beta}{T}\right] \quad , \tag{6}$$

where T is the nuclear temperature in MeV, N is a normalization constant so that $\sum_{\beta} \Gamma_{\beta} = \Gamma$, and B^* is an effective binding energy for the particle. For a neutron, this is the binding energy as given, for example, in the mass tables of Myers and Swiatecki[81]; for a proton or alpha this is the binding energy plus a constant (~ 0.8) times the barrier energy for the particle and the residual nucleus. The value of the constant was determined empirically by comparing the intensities calculated with a trial value (and assuming T = 1.5) with those measured for the ground-band transitions in a doubly-even nucleus in-beam and out-of-beam, as shown in Fig. 19. Here the compound nucleus is ^{128}Ce from ^{16}O + ^{112}Sn, and the gamma-rays of ^{124}Ba seen in-beam come from the 2p2n reaction while their yield out-of-beam is the sum of the 4n and p3n reactions[70]. The same type of evaluation was also performed in the osmium region, and the same value of the constant was obtained.

With this one can now find where $B_n^* = B_p^*$ or $\Gamma_p/\Gamma_n = 1$ throughout this region of the Periodic Table, and this curve is shown in Fig. 20. The black squares indicate the stable nuclei. Obviously one cannot proceed very far beyond this curve (with appreciable cross section) by particle evaporation, as mostly protons will be emitted. However, by the proper choice of heavy-ion projectile and target, the initial compound nucleus formed can be made more neutron deficient. The dashed curve in the figure labeled LCN shows this lightest compound nucleus that can be made by any stable target-projectile pair. Here we are up against a real limit, as an attempt to make still more neutron-deficient nuclei requires neutron evaporation and means going against the exponentially decreasing factor represented by Eq. (6). Two lines to the left of the LCN curve indicate yields of $\leq 10^{-6}$ and $\leq 10^{-12}$ for neutron emission from the lightest compound nucleus, and it

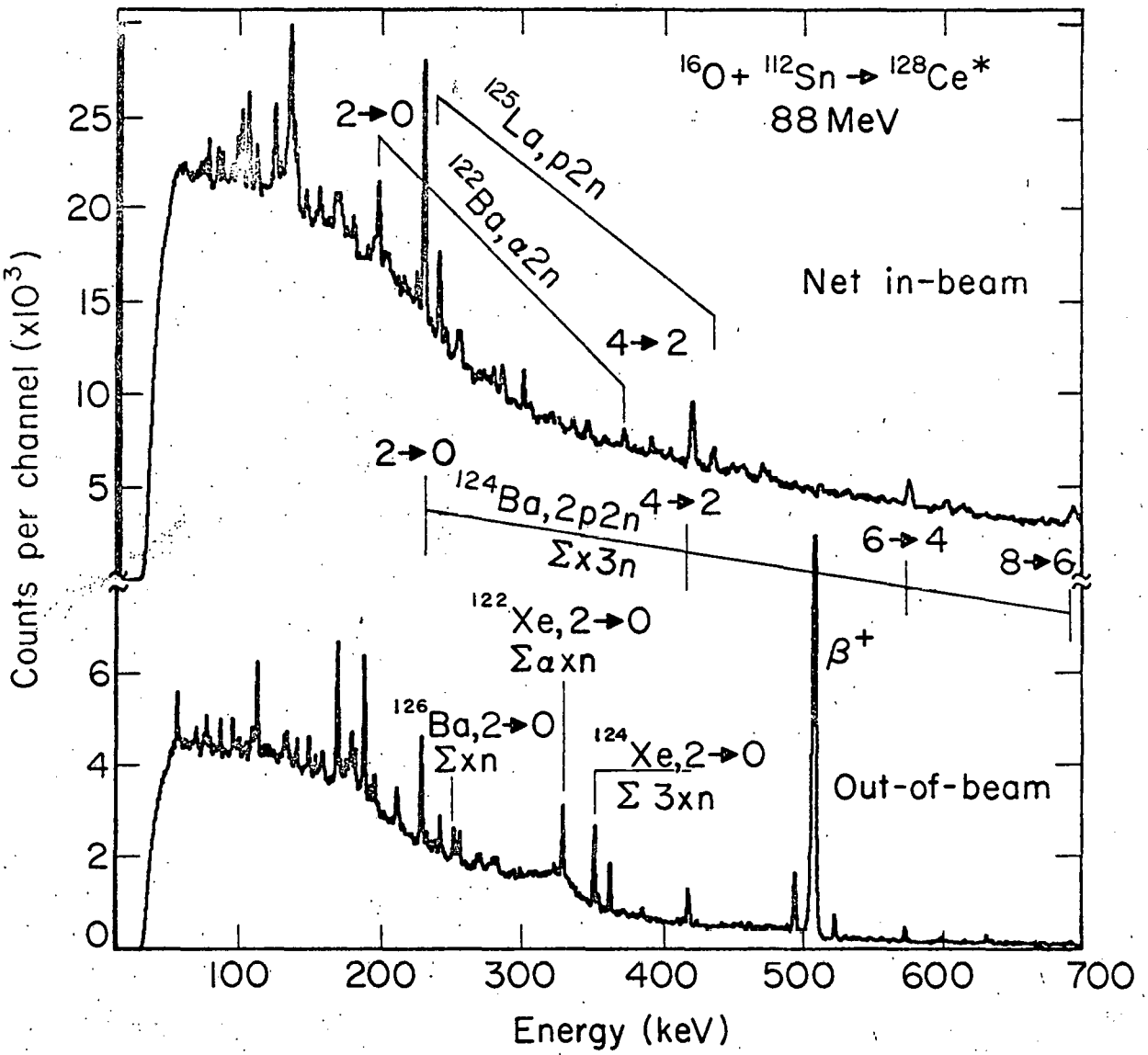

XBL707-3261

Fig. 19

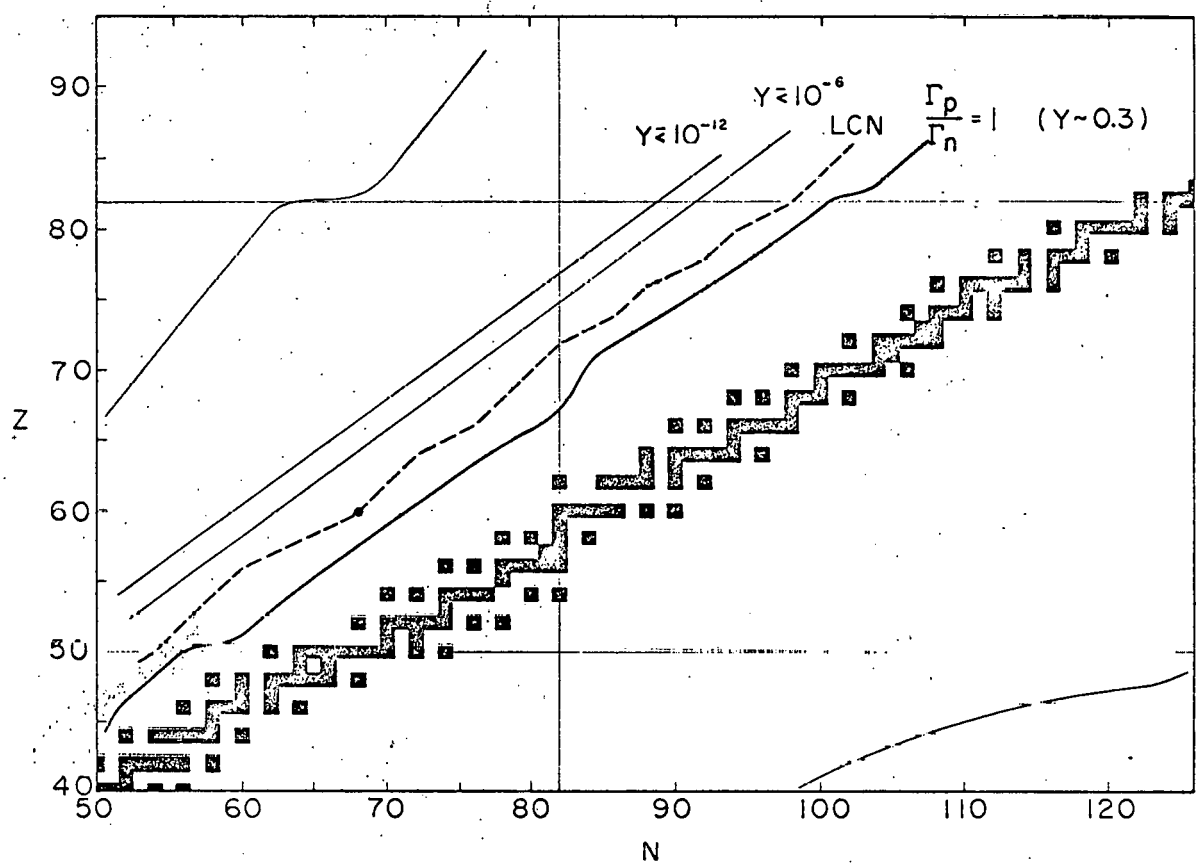
Y≤10⁻¹²
Y≤10⁻⁶
LCN
Γp/Γn = 1 (Y~0.3)
Z
N
90
80
70
60
50
40
50
60
70
80
90
100
110
120
XBL706-3153

Fig. 20

can be seen how rapidly the yield falls off. On this wing of the yield curve one fewer neutron corresponds to a drop in cross section by almost one hundred, and much more sensitive detection methods will be needed. But even with observation of yields of only $10^{-12}\sigma_c$ we would still be only halfway to the proton drip line ($B_p^* = 0$).

It is interesting to note that product nuclei in the region between the curves labeled LCN and $\Gamma_p/\Gamma_n = 1$ can equally well be made by proton emission from the LCN or by neutron emission from a compound nucleus of the product proton number. We have, for example, made ^{126}Ce by these two methods[70], as shown in Fig. 21. The top spectrum shows ^{126}Ce observed in-beam from ^{112}Sn(^{16}O,2n)^{126}Ce and the third spectrum down shows the same transitions in-beam from ^{92}Mo(^{36}Ar,2p)^{126}Ce. In the last reaction ^{128}Nd is the compound nucleus, and is the lightest compound nucleus of Nd possible, we believe, using stable nuclei.

Clearly to make a desired neutron-deficient nucleus as cleanly and in as high a yield as possible, one should involve as few neutron evaporation steps as possible, as at each one there is an increasingly probable chance for proton or alpha emission. Thus to make a light platinum, say ^{178}Pt, by (p,xn) on ^{191}Ir requires 14 neutron evaporation steps, and although neutron emission does dominate at first, Γ_n/Γ is still less than unity and becomes very small for the last steps, leading to a very small yield. P. G. Hansen *et al.*[82], for example, have made ^{180}Hg by lead spallation with 600 MeV protons, and after separation of the Hg isotopes observe the first excited 2+ level in ^{176}Pt from the alpha decay. But the yield of ^{180}Hg is $< 10^{-6} - 10^{-7}$ of the reaction cross section. On the other hand, production of ^{176}Pt by ^{147}Sm(^{32}S,3n) or from ^{144}Sm(^{35}Cl,p2n) should be a significant part of the total compound nucleus cross section, and we have indeed observed the transitions in ^{176}Pt from such in-beam Ge(Li) spectra[83].

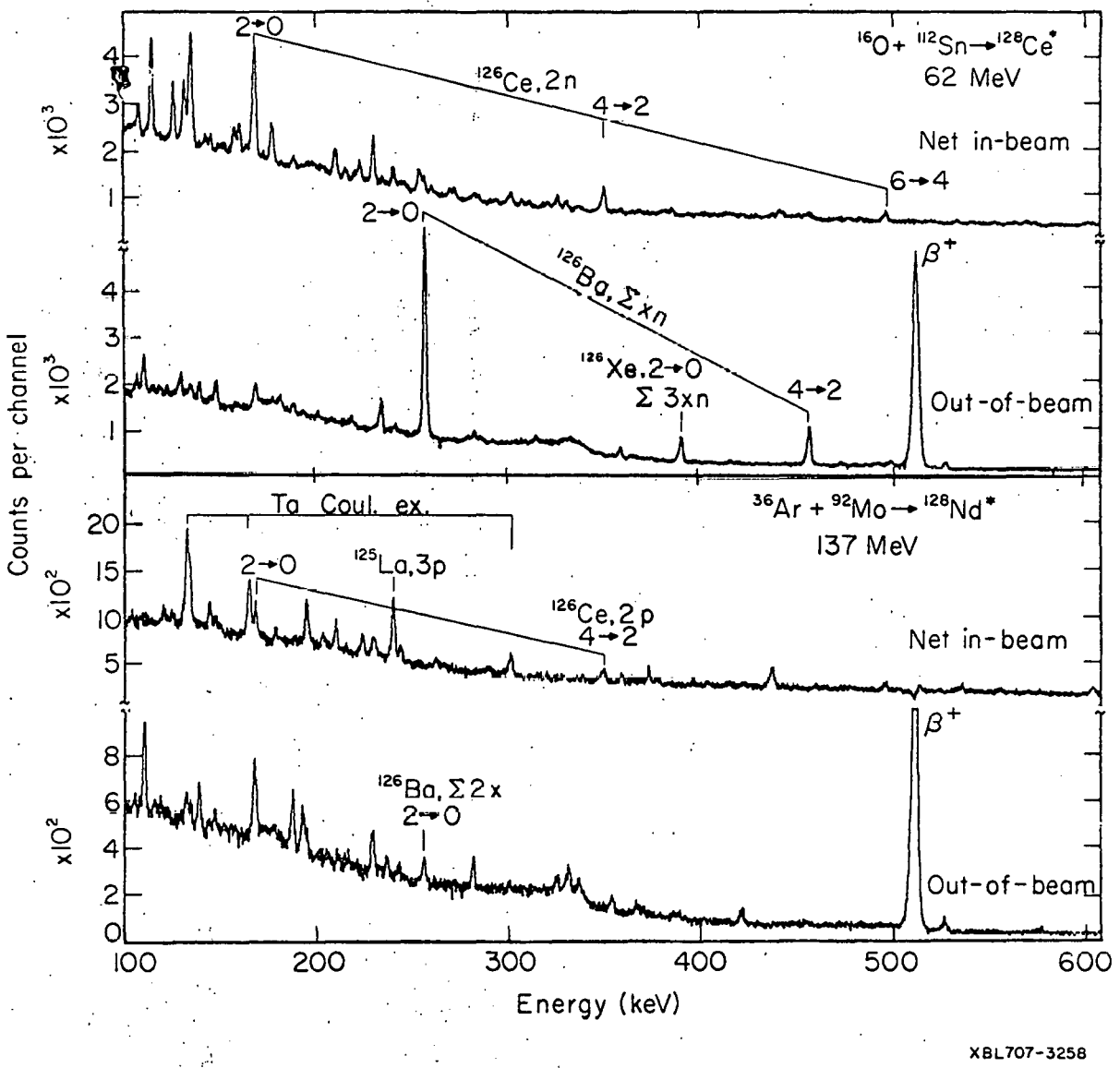
Counts per channel
x10³
x10²
2→0
126Ce, 2n
4→2
6→4
16O+ 112Sn→128Ce*
62 MeV
Net in-beam
126Ba, Σxn
126Xe, 2→0
Σ 3xn
β+
Out-of-beam
Ta Coul. ex.
36Ar + 92Mo→128Nd*
137 MeV
125La, 3p
126Ce, 2p
126Ba, Σ2x
Energy (keV)
XBL707-3258

Fig. 21

In the case just cited, the enormously greater sensitivity given by employment of an isotope separator over the use of a Ge(Li) detector looking at the target in-beam just about equalizes the advantage of the heavy-ion projectile system over proton spallation to form the desired neutron-deficient product. It would seem that union of the two techniques could be a very powerful tool in nuclear spectroscopic studies.

ACKNOWLEDGMENTS

I am grateful to Dr. F. S. Stephens for discussions, calculations, and advice on all the topics covered. I would also like to thank Drs. J. Leigh, H. Maier, J. Quebert, and K. Nakai for help with individual topics.

REFERENCES

1) S. Devons, H. G. Hereward, and G. R. Lindsey, Nature 164, 586 (1949); S. Devons, G. Goldring, and G. R. Lindsey, Proc. Phys. Soc. (London) A, 67, 134 (1954).

2) S. Devons, G. Manning, D. St. P. Bunbury, Proc. Phys. Soc. (London) A, 68, 18 (1955).

3) J. Thirion and V. L. Telegdi, Phys. Rev. 92, 1253 (1953).

4) J. Burde and S. G. Cohen, Phys. Rev. 104, 1093 (1956).

5) J. C. Severiens and S. S. Hanna, Phys. Rev. 104, 1612 (1956).

6) T. K. Alexander and K. W. Allen, Can. J. Phys. 43, 1563 (1965).

7) T. K. Alexander, K. W. Allen, and D. C. Healey, Phys. Letters 20, 402 (1965).

8) P. G. Bizzeti, A. M. Bizzeti-Sona, S. Kalbitzer, and B. Povh, Nucl. Phys. A104, 577 (1967).

9) D. R. Goosman, and R. W. Kavanagh, Phys. Letters 24B, 507 (1967).

10) K. W. Jones, A. Z. Schwarzschild, E. K. Warburton, and D. B. Fossan, Phys. Rev. 178, 1773 (1969).

11) R. M. Diamond, F. S. Stephens, W. H. Nelly, and D. Ward, Phys. Rev. Letters 22, 546 (1969).

12) J. L. Quebert, K. Nakai, R. M. Diamond, and F. S. Stephens, Nucl. Phys. A150, 68 (1970).

13) R. M. Diamond, F. S. Stephens, K. Nakai, and R. Nordhagen, Contributions to International Conference on Properties of Nuclear States (University of Montreal Press, Montreal 1969) p. 7; the slightly revised figures shown here are to be published.

14) F. W. Richter, J. Schütt, and D. Wiegandt, Z. Phys. 213, 202 (1968).

15) P. J. Wolfe and R. P. Scharenberg, Phys. Rev. 160, 866 (1967).

16) D. Ycboah-Amankwah, L. Grodzins, and R. B. Frankel, Phys. Rev. Letters 18, 791 (1967).

17) P. Steiner, E. Gerdan, P. Kienle, and H. J. Körner, Phys. Letters 24B, 515 (1967); P. Kienle, W. Henning, G. Raindl, H. J. Körner, H. Schaller, and F. Wagner, J. Phys. Soc. Japan Suppl. 24, 207 (1962).

18) S. Bernow, S. Devons, I. Duerdoth, D. Hitlin, S. W. Kast, E. R. Macagno, J. Rainwater, K. Runge, and C. S. Wu, Phys. Rev. Letters 18, 787 (1967).

19) F. S. Stephens, D. Ward, R. M. Diamond, J. deBoer, and R. Covello-Moro, to be published.

20) J. L. Quebert, G. Symons, F. S. Stephens, and R. M. Diamond, to be published.

21) A. Winther and J. deBoer, California Institute of Technology Technical Report, 1965 (unpublished), and in "Coulomb Excitation", ed. by K. Alder and A. Winther (Academic Press, New York, 1966) p. 303.

22) F. S. Stephens, R. M. Diamond, N. K. Glendenning, and J. deBoer, Phys. Rev. Letters 24, 1137 (1970).

23) D. L. Hendrie, N. K. Glendenning, B. G. Harvey, O. N. Jarvis, H. H. Duhm, J. Saudinos, and J. Mahoney, Phys. Letters 26B, 127 (1968).

24) G. Breit and J. P. Lazarus, Phys. Rev. 100, 942 (1955); G. Breit, R. L. Gluckstern, and J. E. Russell, Phys. Rev. 103, 722 (1956).

25) J. deBoer and J. Eichler, in "Advances in Nuclear Physics", ed. by M. Baranger and E. Vogt, (Plenum Publishing Co., New York, 1968) Vol. 1, p. 1.

26) A. C. Douglas, W. Bygrave, D. Eccleshall, and M. J. L. Yates, in "Proceedings of the Third Conference on Reactions between Complex Nuclei", ed. by A. Ghiorso, R. M. Diamond, and H. E. Conzett (University of California Press, Berkeley, 1963) p. 274.

27) G. Goldring, J. deBoer, and H. Winkler, in "Proceedings of the Third Conference on Reactions between Complex Nuclei", ed. by A. Ghiorso, R. M. Diamond, and H. Conzett (University of California Press, Berkeley, 1963) p. 278.

28) P. H. Stelson, W. T. Milner, J. L. C. Ford, F. K. McGowan, and R. L. Robinson, Bull. Am. Phys. Soc. 10, 427 (1965).

29) J. deBoer, R. G. Stokstad, G. D. Symons, and A. Winther, Phys. Rev. Letters 14, 564 (1965).

30) R. G. Stokstad, I. Hall, G. D. Symons, and J. deBoer, Nucl. Phys. A92, 319 (1967).

31) J. J. Simpson, D. Eccleshall, M. J. L. Yates, and N. J. Freeman, Nucl. Phys. A94, 177 (1967).

32) D. Cline, P. Jennens, and C. Towsley, to be published (private communication, August, 1970).

33) J. R. Kerns, J. X. Saladin, R. J. Pryor, and S. A. Lane, Bull. Am. Phys. Soc. 14, 1221 (1969).

34) C. Engler, Phys. Rev. 1C, 734 (1970).

35) H. J. Gertzman, D. Cline, H. E. Gove, and P. M. S. Lesser, Nucl. Phys., in press (1970).

36) O. Häuser, B. W. Hooton, D. Pelte, T. K. Alexander, and H. C. Evans, Phys. Rev. Letters 22, 359 (1969); ibid 23, 320 (1969).

37) D. Schwalm and B. Povh, Phys. Letters 29B, 103 (1969).

38) A. Bamberger, P. G. Bizzeti, and B. Povh, Phys. Rev. Letters 21, 1599 (1968).

39) K. Nakai, J. L. Quebert, F. S. Stephens, and R. M. Diamond, Phys. Rev. Letters 24, 903 (1970).

40) K. Nakai, F. S. Stephens, and R. M. Diamond, Nucl. Phys. A150, 114 (1970).

41) E. L. Brady and M. Deutsch, Phys. Rev. 78, 558 (1950).

42) H. Aeppli, H. Albers-Schönberg, A. S. Bishop, H. Frauenfelder, and E. Heer, Phys. Rev. 84, 360 (1951).

43) "Perturbed Angular Correlations", ed. by E. Karlsson, E. Matthias, and K. Siegbahn, (North-Holland Publishers, Amsterdam, 1964).

44) "Hyperfine Structure and Nuclear Radiations", ed. by E. Matthias and D. Shirley (North-Holland Publishers, Amsterdam, 1968).

45) L. Grodzins, in "Annual Review of Nuclear Science", ed. by E. Segre, J. R. Grover, and H. P. Noyes (Annual Reviews, Palo Alto, 1968) p. 291.

46) I. Ben Zvi, P. Gilad, M. Goldberg, G. Goldring, A. Schwarzschild, A. Sprinzak, and Z. Vager, Nucl. Phys. A121, 592 (1968).

47) R. Nordhagen, G. Goldring, R. M. Diamond, K. Nakai, and F. S. Stephens, Nucl. Phys. A142, 577 (1970).

48) L. Grodzins, R. R. Borchers, and G. B. Hagemann, Phys. Letters 21, 214 (1966).

49) F. Boehm, G. B. Hagemann, and A. Winther, Phys. Letters 21, 217 (1966).

50) R. R. Borchers, B. Herskind, J. D. Bronson, L. Grodzins, R. Kalish, and D. E. Murnik, Phys. Rev. Letters 20, 424 (1968).

51) J. Lindhard, Proc. Roy. Soc. (London) A311, 11 (1969).

52) G. Goldring, R. Kalish, and H. Spehl, Nucl. Phys. 80, 33 (1966).

53) G. Goldring, in "Hyperfine Structure and Nuclear Radiations", ed. by E. Matthias and D. Shirley (North-Holland Publishers, Amsterdam, 1968) p. 640.

54) I. Ben Zvi, P. Gilad, G. Goldring, P. Hillman, A. Schwarzschild, and Z. Vager, Nucl. Phys. A109, 201 (1968).

55) H. J. Körner, J. Braunsfurth, H. F. Nesemann, S. J. Skorka, and B. Zeitnitz, "Compt. Rend. Congr. Int. Phys. Nucl.," ed. by P. Gugenberger, (Paris, 1964) Vol. II, p. 478.

56) H. Schmidt, J. Morgenstern, H. J. Körner, J. Braunsfurth, and S. J. Skorka, Phys. Letters 24B, 457 (1967).

57) J. Bleck, D. W. Haag, W. Leitz, and W. Ribbe, Phys. Letters 26B, 134 (1968).

58) T. Yamazaki and E. Matthias, Phys. Rev. 175, 1476 (1968).

59) T. Yamazaki, T. Nomura, T. Katoh, T. Inamura, A. Hashizume, and T. Tendo, Phys. Rev. Letters 24, 317 (1970).

60) H. Maier, F. S. Stephens, K. Nakai, and R. M. Diamond, to be published.

61) J. Christiansen, H.-E. Mahnke, E. Recknagel, D. Riegel, G. Weyer, and W. Witthuhn, Phys. Rev. Letters 21, 554 (1968).

62) K. Sugimoto, A. Mizobuchi, K. Nakai, and K. Matuda, Phys. Letters 18, 381 (1965).

63) D. Quitman, J. M. Jaklevic, and D. A. Shirley, Phys. Letters 30B, 329 (1969).

64) H. Morinaga and P. C. Gugelot, Nucl. Phys. 46, 210 (1963).

65) G. B. Hansen, B. Elbek, K. A. Hagemann, and W. F. Hornyak, Nucl. Phys. 47, 529 (1963).

66) M. Sakai, T. Yamazaki, and H. Ejiri, Nucl. Phys. 74, 81 (1965).

67) F. S. Stephens, N. L. Lark, and R. M. Diamond, Nucl. Phys. 63, 82 (1965).

68) J. R. Grover and J. Gilat, Phys. Rev. 157, 802 (1967); ibid 814; ibid 823; J. R. Grover, Phys. Rev. 157, 832 (1967).

69) J. O. Newton, F. S. Stephens, R. M. Diamond, W. H. Kelly, and D. Ward, Nucl. Phys. A141, 631 (1970).

70) F. S. Stephens, J. R. Leigh, and R. M. Diamond, to be published; D. Ward, R. M. Diamond, and F. S. Stephens, Nucl. Phys. A117, 309 (1968).

71) J. B. Wilhelmy, S. G. Thompson, R. C. Jared, and E. Cheifetz, submitted for publication.

72) J. M. Jaklevic, C. M. Lederer, and J. M. Hollander, Phys. Letters 29B, 179 (1968).

73) G. Scharff-Goldhaber and J. Weneser, Phys. Rev. 98, 212 (1955).

74) J. O. Newton, Nucl. Phys. A108, 353 (1968).

75) A. K. Kerman, Dan. Mat. Fys. Medd. 30, No. 15 (1956).

76) A. Bohr and B. Mottelson, "Nuclear Structure", Vol. II, to be published.

77) R. M. Diamond, J. Leigh, and F. S. Stephens, to be published.

78) S. A. Hjorth, H. Ryde, K. A. Hagemann, G. Løvhøiden, and J. C. Waddington, Nucl. Phys. A144, 513 (1970).

79) F. S. Stephens, in "Proceedings of the International Conference on Properties of Nuclear States", ed. by M. Harvey (University of Montreal Press, Montreal, 1969) p. 127; to be published.

80) J. R. Leigh, F. S. Stephens, and R. M. Diamond, to be published.

81) W. D. Myers and W. J. Swiatecki, Lawrence Radiation Laboratory Report UCRL-11980 (May, 1965).

82) P. G. Hansen, H. L. Nielsen, K. Wilsky, M. Alpsten, M. Finger, A. Lindahl, R. A. Naumann, and O. B. Nielsen, Nucl. Phys. A148, 249 (1970).

83) J. R. Leigh, F. S. Stephens, and R. M. Diamond, to be published.

FIGURE CAPTIONS

Fig. 1. Schematic view of a recoil-distance Doppler-shift method used for measuring lifetimes.

Fig. 2. Spectra from ^{152}Sm Coulomb excited with back-scattered ^{40}Ar projectiles. The lead plunger-target distance is indicated on each spectrum. Positions of the unshifted (shifted) lines are given at the top (bottom) of the figure.

Fig. 3. Semi-log plot of unshifted fraction of each transition in ^{152}Sm vs target-plunger distance. Curves are the calculated best fits allowing for one stage of feeding.

Fig. 4. Possible pathways for exciting the 4+ state. Double arrows indicate Coulomb excitation; single arrows indicate gamma-ray transitions.

Fig. 5. Relationship between E4 moment and a) the back-scatter cross section for populating the 4+ state of ^{152}Sm with 10.4 MeV ^{4}He ions normalized to the case of zero E4 moment, and b) the deformation parameter, β_4, using a radius of $R_0 = 1.2A^{1/3}$ F and a β_2 which yields the experimental E2 moment.

Fig. 6. The static quadrupole moments for the first excited 2+ states of the even-even isotopes of barium[31,33], cerium[34], neodymium[35], and samarium[32]. The solid-dashed and dot-dashed lines correspond to the static moments derived from the measured $B(E2;0^+ \rightarrow 2^+)$ assuming a prolate rigid spheroidal rotor model. This figure is from Ref. 32.

Fig. 7. Intrinsic quadrupole moments, Q_0, in s-d shell nuclei: ⊙ Ref. 39, ❂ Ref. 36, ○ Refs. 37 and 38, □ values calculated from measured $B(E2; 0^+ \rightarrow 2^+)$ values, ◆ odd-A moments deduced from the spectroscopic moment.

Fig. 8. The spectrum of the 123 μsec 7- isomer in ^{206}Pb taken between Hilac beam pulses (20 μsec repetition rate).

Fig. 9. Plot of $\frac{Y(20°) - Y(-70°)}{Y(20°) + Y(-70°)}$ vs time for the 516 keV transition from the 7- isomer in ^{206}Pb.

Fig. 10. Plot of $\frac{Y(T/4;\ 45°)}{Y(3T/4;\ 45°)} / \frac{Y(T/4;\ -45°)}{Y(3T/4;\ -45°)}$ for the 516 keV transition from the 7- isomer in ^{206}Pb from the two counters fixed at ± 45° to the beam direction vs the magnetic field. The two count intervals are centered at T/4 and 3T/4 where T is the repetition time for the pulsed beam.

Fig. 11. Energy levels in the cerium isotopes. The neutron-deficient nuclei are from Ref. 70 and the neutron-excess ones from Ref. 71.

Fig. 12. Energy levels in the 50-neutron nuclei, ^{92}Mo and ^{94}Ru. From Ref. 72.

Fig. 13. Ratios of energies of 4+ to 2+ states vs proton number for various neutron numbers. The neutron-excess nuclei are from Ref. 71.

Fig. 14. Ratios of energies of 4+ to 2+ states vs neutron number for various proton numbers.

Fig. 15. Energy levels in ^{157,159,161,165}Ho. From Ref. 77.

Fig. 16. Plot of $E_{I+1} - E_I/2(I+1)$ vs $4(I+1)^2$ for ^{165}Ho and ^{157}Ho; constant apparent values of A (intercept on ordinate), B/2 (slope), and magnitude of oscillations in energy levels.

Fig. 17. Partial level scheme in ^{157,159}Er (Ref. 79) and in ^{161,163,165}Er (Ref. 78).

Fig. 18. Partial level scheme in ^{160,162}Ho (Ref. 80).

Fig. 19. The in-beam (top) and out-of-beam (bottom) gamma-ray spectra obtained with ^{112}Sn + ^{16}O (88 MeV). The transitions in ^{124}Ba seen in-beam come from the 2p2n reaction, while the yield out-of-beam is the sum of 4n and p3n.

Fig. 20. Partial region of the Periodic Table, with stable isotopes as filled squares and outermost curves of zero effective binding energy, $B^* = 0$. Curve labeled $\Gamma_p/\Gamma_n = 1$ is where neutron and proton emission is calculated to be equally likely, and one labeled LCN is the lightest compound nucleus that can be made with any stable projectile-target combination. Lines with $Y \leqslant 10^{-6}$ and $Y \leqslant 10^{-12}$ give corresponding yields for neutron emission from LCN.

Fig. 21. In order from top to bottom are gamma-ray spectra obtained in- and out-of-beam for $^{112}Sn + ^{16}O$ (62 MeV) and in- and out-of-beam for $^{92}Mo + ^{36}Ar$ (137 MeV).

TECHNICAL INFORMATION DIVISION
LAWRENCE RADIATION LABORATORY
UNIVERSITY OF CALIFORNIA
BERKELEY, CALIFORNIA 94720